J. Fluid Mech. (2021), *vol*. 906, A9. © The Author(s), 2020.
Published by Cambridge University Press
doi:10.1017/jfm.2020.762

On the starting vortex generated by a translating and rotating flat plate

D. I. Pullin[1],† **and John E. Sader**[2,3]

[1]Graduate Aerospace Laboratories, California Institute of Technology, Pasadena, CA 91125, USA

[2]ARC Centre of Excellence in Exciton Science, School of Mathematics and Statistics, University of Melbourne, Victoria 3010, Australia

[3]Department of Physics, California Institute of Technology, Pasadena, CA 91125, USA

(Received 21 April 2020; revised 22 July 2020; accepted 8 September 2020)

We consider the trailing-edge vortex produced in an inviscid fluid by the start-up motion of a two-dimensional flat plate. A general starting motion is studied that includes the initial angle-of-attack of the plate (which may be zero), individual time power laws for plate translational and rotational speeds and the pivot position for plate rotation. A vortex-sheet representation for a start-up separated flow at the trailing edge is developed whose time-wise evolution is described by a Birkhoff–Rott equation coupled to an appropriate Kutta condition. This description includes convection by the outer flow, rotation and vortex-image self-induction. It admits a power-law similarity solution for the (small-time) primitive vortex, leading to an equation set where each term carries its own time-wise power-law factor. A set of four general plate motions is defined. Dominant-balance analysis of this set leads to discovery of three distinct start-up vortex-structure types that form the basis for all vortex motion. The properties of each type are developed in detail for some special cases. Numerical and analytical solutions are described and transition between solution types is discussed. Singular and degenerate vortex behaviour is discovered which may be due to the absence of fluid viscosity. An interesting case is start-up motion with zero initial angle of attack coupled to power-law plate rotation for which time-series examples are given that can be compared to high Reynolds number viscous flows.

Key words: vortex dynamics, vortex shedding

1. Introduction

The form of the trailing-edge vortex generated when a flat-plate airfoil is accelerated from rest is a classic flow problem in fluid mechanics (Prandtl 1924). For two-dimensional inviscid flow, Wagner (1925) developed a linear theory describing flat-plate starting flow at small angles of attack. But linear theory cannot generally describe the true starting vortex at sufficiently small times for a finite initial angle of attack. A nonlinear similarity description was developed by Anton (1939) (see also Anton 1956) who modelled the true starting vortex in an inviscid fluid by a vortex sheet whose growth – for impulsive start up at a finite angle of attack – followed a 2/3-power suggested earlier by Kaden (1931).

† Email address for correspondence: dpullin@caltech.edu

For starting flow past a semi-infinite plate, improvements and refinements were made by Wedemeyer (1961), Blendermann (1967) and Pullin (1978), while Rott (1956) developed an analytical solution based on a single-vortex-cut model. Tchieu & Leonard (2011) analysed a discrete-vortex model for the arbitrary motion of a finite-chord thin airfoil based on impulse conservation. They found point-vortex motion parallel to the plate at the trailing edge. Regularized vortex blob and vortex particle methods have been applied to the flat-plate start-up in various settings by Koumoutsakos & Shiels (1996), Krasny (1991), Jones (2003), Eldredge (2007), Michelin, Smith & Llewellyn (2009) and others.

Experimental studies of the starting vortex at the trailing edge include Pierce (1961), Pullin & Perry (1980) and Auerbach (1987). These show a viscous starting vortex for a flat plate whose centre initially moves nearly normal to the plate near the edge of separation. Luchini & Tognaccini (2002) reported numerical Navier–Stokes solutions of viscous starting flow about a semi-infinite plate in the self-similar reference frame suggested by inviscid theory. They identified several flow stages that include the formation of an attached, viscous Rayleigh layer at very early times, followed by a period of self-similar vortex growth, after which finite-plate geometry modifies the growth profile. Nitsche & Xu (2014) and Xu & Nitsche (2015) confirmed these findings and investigated the detailed scaling and duration of the self-similar growth period. At sufficiently large Reynolds number, both experimental (Pierce 1961) and some viscous simulations (Koumoutsakos & Shiels 1996; Luchini & Tognaccini 2002) show shear-layer instabilities on the separating spiral shear layer. Luchini & Tognaccini (2017) compared these motions with their counterpart found in inviscid starting-vortex simulations. Xu, Nitsche & Krasny (2017) made detailed comparisons of regularized, inviscid spiral-like solutions with viscous simulations for the impulsive, non-rotating starting flow of a finite flat plate at Reynolds numbers between 250 and 2000. Good agreement was reported for large-scale features of the flow.

We consider the trailing-edge vortex produced in an inviscid, incompressible fluid by the start-up motion of a two-dimensional flat plate. The plate moves with general and prescribed start-up kinematics with respect to a laboratory frame. This is described by parameters that include independent power-law translational velocity and rotational angular velocity time dependencies and an arbitrary initial angle of attack that includes zero angle. The centre of rotation may be any fixed point on the plate. This general starting motion will be seen to produce a surprisingly diverse set of starting vortices whose qualitative and quantitative structures vary within the kinematic parameter space.

Our focus is strictly on the 'primitive' start-up vortex at the trailing edge. By this we mean the unique vortex structure produced at sufficiently small but positive times after commencement of the plate starting motion in an inviscid fluid, that cancels the velocity singularity at the plate edge. Later corrections to the vortex shape and trajectory caused by increasingly strong interaction with the global outer flow are not considered. The leading edge is expected to exert no influence on the primitive trailing-edge vortex, as demonstrated for a flat plate with no rotation (Pullin & Wang 2004), and is ignored.

In § 2, we define the plate start-up motion and analyse the singular form of the attached-flow velocity field near the trailing edge. Section 3 develops a vortex-sheet model whose dynamics is defined by a Birkhoff–Rott equation (Rott 1956; Birkhoff 1962; Saffman 1992) in a way that satisfies a Kutta condition that the fluid velocity at the trailing edge remains finite. A time power-law similarity solution is presented in § 4 that involves *a priori* unknown powers of time for both the vortex profile and circulation growth. Using dominant balance for infinitesimally small dimensionless time (appropriate for the primitive vortex), these powers are calculated for the four most general plate start-up motions in § 5. This includes a discussion of degenerate behaviour for vanishing

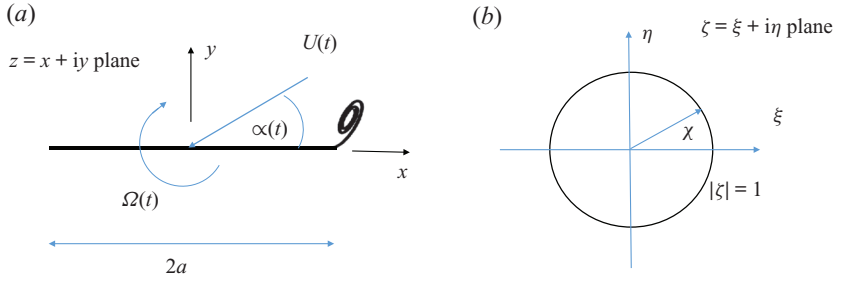

FIGURE 1. (*a*) Schematic of flat rigid plate in starting flow, showing cartoon of the trailing-edge starting vortex. Rotation is about the plate centre, i.e. $d = 0$, and plate translation is at finite angle of attack, $\alpha(t)$. The z-plane is fixed to the moving frame of the plate. (*b*) Unit circle in the $\zeta = \xi + \mathrm{i}\eta$ plane, used to calculate the starting vortex.

plate rotation. The most detailed case analysed is start-up motion with zero initial angle of attack with rotation away from the three-quarter chord point. In § 6, time-series snap shots are provided for the special case of start-up motion with uniform linear acceleration, zero initial angle of attack but with finite rotational angular velocity. These can be directly compared to high Reynolds number viscous flows, with the corresponding limits considered in § 7. Finally, discussion and conclusions are presented in § 8.

Table 1 summarizes all vortices generated by the four general plate motions, which are the principal findings of this study.

2. Start-up motion for a two-dimensional translating and rotating plate

The problem is formulated in the moving (non-inertial) frame of the flat and rigid two-dimensional plate; the Cartesian coordinates (x, y) are referenced to this frame. The plate is immersed in an unbounded inviscid fluid and located at

$$\{(x, y) \mid -a(1+d) \le x \le a(1-d) \text{ and } y = 0\}, \tag{2.1}$$

where the plate length is $2a$ and d specifies the rotational pivot point. For $t > 0$, the plate moves in the (fixed) laboratory frame with linear translational speed, $U(t)$, directed at angle of incidence, $\alpha(t)$, with respect to the plate surface; see figure 1. The initial angle of attack is $\alpha_0 = \alpha(t = 0)$, where $0 \le \alpha_0 < \pi/2$; we note that $\alpha_0 = 0$ is included. The trailing edge is located at $(x, y) = (a[1-d], 0)$ where the distance, ad, is the offset of the pivot point from the half-chord point. Rotation about the three-quarter chord point corresponds to $d = 1/2$. The rotational (angular) speed of the plate in the laboratory frame is $\Omega(t)$, which is taken as positive in the clockwise direction.

We are interested in the initial motion of the primitive start-up vortex shed at the plate trailing edge, i.e. for very small times. In the presence of both translational and rotational plate motion, this will be seen to produce novel classes of starting-vortex solutions.

2.1. *Inviscid attached flow*

The streamfunction for attached flow and $d = 0$ is developed in Milne-Thomson (1996) § 9.63, page 258. For general d, in the (non-inertial) frame of reference, the streamfunction

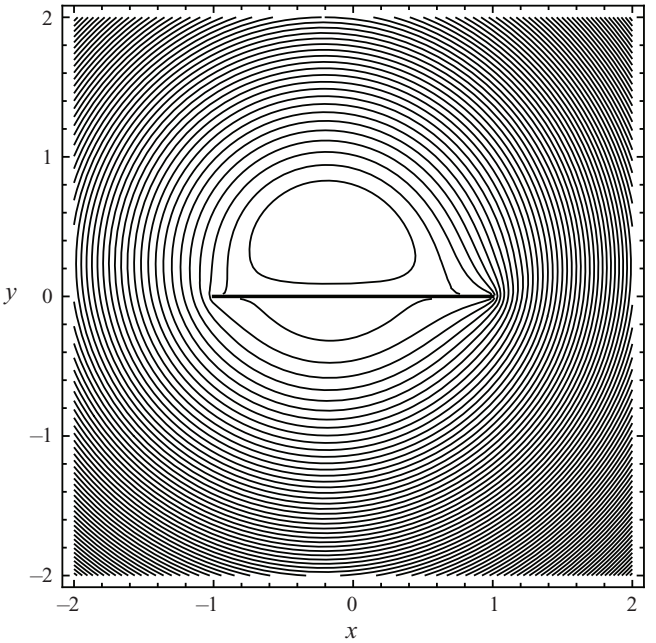

FIGURE 2. Streamlines generated by a flat rigid plate with $a = 1$, $U = 1$, $\Omega = 3$, $d = 0$ and $\alpha = \pi/4$, corresponding to a plate of length 2, instantaneous translational speed of 1, rotating with instantaneous angular speed of 3, pivot point at the plate centre and instantaneous angle of attack of $\pi/4$, respectively. Streamlines shown in reference frame of the moving plate.

can be written as

$$\psi(x, y, t) = \mathrm{Im}\{W_a(z, t)\} - \tfrac{1}{2}\Omega(t)(x^2 + y^2), \tag{2.2}$$

where $z = x + \mathrm{i}y$ with i being the imaginary unit, and

$$W_a(z, t) = \frac{A(t)}{\zeta} + \frac{B(t)}{\zeta^2} + U(t)(z + ad)\exp(-\mathrm{i}\alpha(t)), \tag{2.3a}$$

$$A(t) = \mathrm{i}a[-a\Omega(t)d + U(t)\sin(\alpha(t))], \quad B(t) = \frac{\mathrm{i}}{4}\Omega(t)a^2, \tag{2.3b}$$

$$\zeta(z) = \frac{z}{a} + d + \left(\frac{z}{a} + d - 1\right)^{1/2}\left(\frac{z}{a} + d + 1\right)^{1/2}, \tag{2.3c}$$

where the time dependence is due only to the plate's kinematics in this inviscid formulation. The subscript of W_a refers to attached flow, $\zeta(z)$ maps the exterior of the flat plate located at $C \equiv \{z = x + \mathrm{i}y \,|\, -a(1 + d) \le x \le a(1 - d) \text{ and } y = 0\}$, to the exterior of the unit circle, $\mathcal{C} \equiv \{\zeta = \xi + \mathrm{i}\eta \,|\, |\zeta| = 1\}$. An appropriate branch can be defined by a cut connecting the branch points, $z = (-a[1 + d], 0)$ and $(a[1 - d], 0)$. The points, $\zeta = (-1, 0)$ and $(1, 0)$, map to the plate edges at $z = (-a[1 + d], 0)$ and $(a[1 - d], 0)$, respectively. On $\mathcal{C}$, $\zeta = \exp(\mathrm{i}\chi)$ maps to the plate surface, $z = a(\cos\chi - d)$. It is easily verified that on the plate, the streamfunction is $\psi = -\frac{1}{4}a^2\Omega(1 + 2d^2)$ which depends on time only. Streamlines are shown in figure 2 for translational speed, $U = 1$, angular speed, $\Omega = 3$, pivot position at the plate centre, $d = 0$ and angle of attack, $\alpha = \pi/4$.

In the translating and rotating reference frame of the plate, the velocity components at a field point, z, can be written as

$$u - \mathrm{i}v = \frac{\mathrm{d}W_a}{\mathrm{d}z} - \mathrm{i}\Omega\bar{z}, \tag{2.4}$$

where the overline denotes the complex conjugate. The vorticity is zero.

In this reference frame, the x and y fluid velocity components at the plate surface are, respectively,

$$u = \frac{a\Omega[d\cos\chi - \frac{1}{2}\cos(2\chi)] - U\sin(\alpha - \chi)}{\sin\chi}, \quad v = 0. \tag{2.5a,b}$$

Generally, u is singular at the plate trailing edge $\chi = 0$ (i.e. $z = a[1 - d]$) and leading edge $\chi = \pi$ (i.e. $z = -a[1 + d]$). A stagnation point on the plate surface occurs when $u = 0$, giving

$$a\Omega[d\cos\chi - \tfrac{1}{2}\cos(2\chi)] - U\sin(\alpha - \chi) = 0. \tag{2.6}$$

When $d = 0$, $U = 0$, $\Omega \neq 0$ (pure rotation about the plate centre), stagnation points occur at $\cos(2\chi) = 0$ and so $\chi = \pi/4,\ 3\pi/4,\ 5\pi/4,\ 7\pi/4$. This corresponds to $x = \pm a/\sqrt{2}$, $y = 0^+$ and 0^-, in agreement with Milne-Thomson (1996).

2.2. *Attached flow near the trailing edge*

The function, $W_a(z, t)$, has a $(z/a + d - 1)^{1/2}$ singularity at the trailing edge, $z = a(1 - d)$, where for attached flow, the fluid velocity and pressure are both singular. We consider spatial points near $z = a(1 - d)$ and write

$$z = a(1 - d) + \hat{z}, \quad \hat{z} = \hat{x} + \mathrm{i}\hat{y} = r\exp(\mathrm{i}\theta), \tag{2.7a,b}$$

where $r = \sqrt{\hat{x}^2 + \hat{y}^2}$ and $\theta \in [-\pi, \pi)$ is the angle made by $\hat{z}$ with the positive $\hat{x}$-axis. Expanding $W_a(z, t)$ for small r, and any term that is purely a function of time (including constants), gives

$$\begin{aligned} W_a(\hat{z}) = -2\,i\left(\frac{a}{2}\right)^{1/2}\hat{z}^{1/2}\left(a\Omega\left[\frac{1}{2} - d\right] + U\sin\alpha\right) \\ + \hat{z}\,(\mathrm{i}a\Omega[1 - d] + U\cos\alpha) + O(\hat{z}^{3/2}). \end{aligned} \tag{2.8}$$

The branch cut for $\hat{z}^{1/2}$ extends from $\hat{z} = 0$ along the negative $\hat{x}$ axis, i.e. along the plate. Using (2.4), the complex velocity for the attached flow (again denoted with subscript, a) near the trailing edge is

$$u_a - \mathrm{i}v_a = -\mathrm{i}\left(\frac{a}{2}\right)^{1/2}\hat{z}^{-1/2}\left(a\Omega\left[\frac{1}{2} - d\right] + U\sin\alpha\right) + U\cos\alpha + O(|\hat{z}|^{1/2}). \tag{2.9}$$

For rotation about the three-quarter chord point, $d = 1/2$, the rotational contribution to (2.9) vanishes. More generally, it can be seen that the coefficient of $\hat{z}^{-1/2}$ is zero when $a\Omega(1/2 - d) + U\sin\alpha = 0$. Streamlines for a flow with this property are shown in figure 3 for translational speed, $U = 3/(2\sqrt{2})$, angular speed, $\Omega = 3$, rotation about the three-quarter chord point, $d = 1/2$, and angle of attack, $\alpha = \pi/4$. The plate lies on the interval, $-3/4 \leq x \leq 1/4$ and $y = 0$. It can be seen that there is smooth flow off the trailing edge, $z = x + \mathrm{i}y = 1/4$. This condition will be instantaneous at $t = 0^+$.

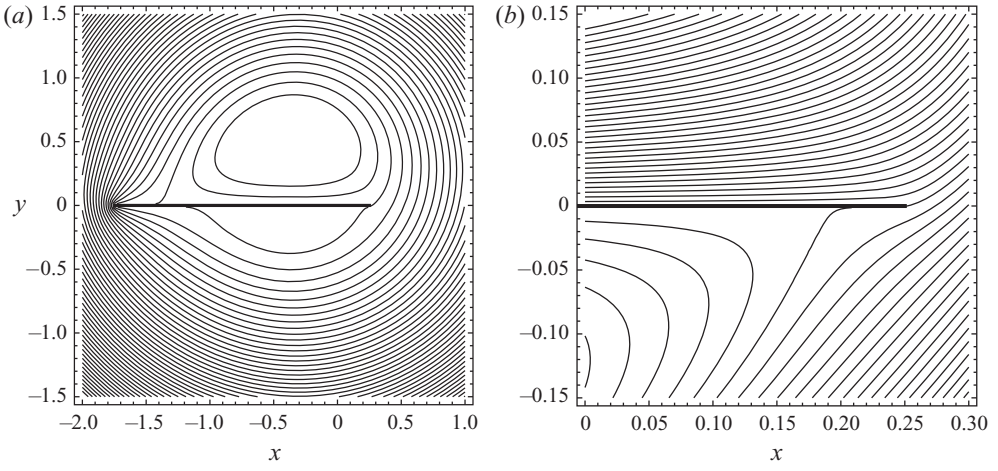

FIGURE 3. Streamlines generated by a flat rigid plate with $a = 1$, $U = 3/(2\sqrt{2})$, $\Omega = 3$, $d = 1/2$ and $\alpha = \pi/4$. (*a*) Full-plate view. (*b*) Close up near trailing edge. These parameters are similar to those used for the flow in figure 2, except the plate now rotates about its three-quarter chord point (rather than its centre) and has a translational speed of $U = 3/(2\sqrt{2}) \approx 1.06$ (rather than 1). Streamlines again shown in the moving reference frame of the plate.

2.3. *Power law in time motion of the plate*

We consider a plate whose respective translational and rotational speeds are

$$U(T) = U_0 T^m, \quad \Omega(T) = \Omega_0 T^p, \tag{2.10a,b}$$

where $U_0 > 0$ and $\Omega_0 > 0$ are the (constant) characteristic translational and angular velocity scales, respectively, and dimensionless time is

$$T = \frac{tU_0}{a}. \tag{2.11}$$

The constants, $m \geq 0$ and $p \geq 0$, in (2.10*a*,*b*) are key control parameters of the plate motion that specify its translational and rotational time dependencies, respectively.

The instantaneous angle of attack, $\alpha(T)$, of the plate directly follows from (2.10*a*,*b*),

$$\alpha(T) = \alpha_0 + \frac{\beta}{1+p} T^{1+p}, \tag{2.12}$$

where α_0 is the initial angle of attack. The constant parameter,

$$\beta = \frac{\Omega_0 a}{U_0}, \tag{2.13}$$

specifies the relative rotational-to-translational plate motion.

Impulsive pure rectilinear motion at constant angle of attack, $\alpha(t) = \alpha_0$, corresponds to $m = 0$ (giving $U = U_0 > 0$) and $\Omega_0 \to 0$ (Prandtl 1924); this widely studied case is discussed in § 5.6.

3. Vortex-sheet representation of separated flow

As $\hat{z} \to 0$, the attached-flow velocity becomes singular, varying as $r^{-1/2}$ away from the trailing edge where r is distance from this edge; see (2.7*a*,*b*). This can be removed by modelling boundary-layer separation using either a vortex-sheet or a cut-point-vortex system emerging from $\hat{z} = 0$ for $t > 0$. Presently, we utilize a vortex-sheet model. Our aim is to analyse the vortex structure in the $(m, p, \alpha_0, d, \beta)$ parameter space corresponding to the translational power law, rotational power law, initial angle of attack, pivot position and relative strength of plate rotation to translation, respectively.

3.1. *Self-induced velocity of vortex sheet*

In the complex z-plane, we describe the separated vortex-sheet position and motion by the function $\hat{z} = \hat{z}_v(\Gamma, t)$, where Γ is a Lagrangian-like variable that measures the total amount of circulation between a point on the vortex sheet and its free edge; the subscript v refers to the vortex sheet. For a material point on the sheet, moving with the average of the field velocities on either side of the sheet, Γ is conserved. The dynamical motion of the sheet is described by the Eulerian–Lagrangian Birkhoff–Rott equation (Rott 1956; Birkhoff 1962; Saffman 1992)

$$\left(\frac{\partial \bar{\hat{z}}_v}{\partial t}\right)_{\Gamma} = u_a - \mathrm{i}v_a + u_v - \mathrm{i}v_v, \tag{3.1}$$

where $u_v - \mathrm{i}v_v$ is the self-induced, sheet-image velocity that satisfies the boundary condition on the plate, guaranteeing total circulation of the vortex–plate system is zero. Using the image-circle theorem (Milne-Thomson 1996) to construct an image system in the circle in the ζ-plane, that satisfies the boundary condition of zero normal velocity on the flat plate with zero total circulation, this velocity contribution can be expressed as

$$u_v - \mathrm{i}v_v = -\left(\frac{\mathrm{d}\zeta}{\mathrm{d}z}\right)_{\hat{z}_v} \frac{1}{2\pi\mathrm{i}} \int_{\Gamma_0(t)}^{0} \left(\frac{1}{\zeta_v - \zeta_v'} - \frac{1}{\zeta_v - \dfrac{1}{\bar{\zeta}_v'}}\right) \mathrm{d}\Gamma', \tag{3.2}$$

where $\zeta_v(\Gamma, t) = \zeta(z_v(\Gamma, t))$ is the vortex-sheet curve in the ζ-plane given by (2.3*c*) and $\zeta_v' = \zeta(z_v(\Gamma', t))$. In (3.2), the integral denotes the Cauchy principal value. The upper limit of integration corresponds to the vortex-sheet free edge which is the point on the sheet that began the separation at $t = 0$; the lower limit of $\Gamma_0(t)$ is the total circulation shed at time $t > 0$ and coincides with the plate trailing edge. The first term inside the integral represents the self-induction of the shed vortex sheet while the second term is the complex velocity induced by the image vortex sheet, or 'bound' circulation.

Using (2.3*c*) to expand the integrand in (3.2) to leading order for $|\hat{z}_v| \ll a$, and substituting the result and (2.9) into (3.1), gives the required dynamical equation describing the vortex-sheet motion to $O(\hat{z}_v^{1/2})$,

$$\left(\frac{\partial \bar{\hat{z}}_v}{\partial t}\right)_{\Gamma} = U\cos\alpha - \mathrm{i}\left(\frac{a}{2}\right)^{1/2} \hat{z}_v^{-1/2} \left(a\Omega\left[\frac{1}{2} - d\right] + U\sin\alpha\right)$$
$$- \frac{1}{4\pi\mathrm{i}} z_v^{-1/2} \int_{\Gamma_0(t)}^{0} \left(\frac{1}{z_v^{1/2} - z_v'^{\,1/2}} - \frac{1}{z_v^{1/2} + \bar{z}_v'^{\,1/2}}\right) \mathrm{d}\Gamma'. \tag{3.3}$$

The Kutta condition, that the complex velocity at the plate edge is always finite, can be obtained by taking the limit, $\hat{z}_v \to 0$. Requiring that the coefficient of the singular term on the right-hand side vanishes then gives

$$\frac{1}{4\pi}\int_{\Gamma_0(t)}^{0}\left(\frac{1}{z_v{}^{1/2}}+\frac{1}{\overline{z_v}^{1/2}}\right)\mathrm{d}\Gamma+\left(\frac{a}{2}\right)^{1/2}\left(a\Omega\left[\frac{1}{2}-d\right]+U\sin\alpha\right)=0. \tag{3.4}$$

It can be seen that both (3.3) and (3.4) contain the term, $a\Omega[\frac{1}{2}-d]+U\sin\alpha$, where the time dependence of Ω, U and α have been omitted. This term is generally non-zero at $t=0$. However, if it vanishes at $t=0$, then for non-zero $U(t)$, it cannot remain at zero for all $t>0$. The special limiting case, $\Omega(t)\to 0$ and $\alpha(t)\to 0$, corresponds to no starting vortex because the Kutta condition is automatically satisfied; see § 5.6 for a general discussion of the zero rotation limit.

4. Similarity solution

4.1. *Formulation*

Motivated by specified time dependencies of the plate motion in (2.10*a*,*b*) and (2.12), and hence the flow boundary conditions, we search for similarity solutions for the vortex sheet of the form

$$\frac{\hat{z}_v}{a}=T^q Z(\lambda),\quad \lambda=1-\frac{1}{\mathcal{J}T^s}\frac{\Gamma}{U_0 a}, \tag{4.1a,b}$$

where $q\geq 0$ and $s\geq 0$ are additional power-law constants and $\mathcal{J}$ is a dimensionless constant related to the total shed circulation (see (4.3)), all of which are to be determined. The form of the second equation in (4.1*a*,*b*) is now justified.

In (4.1*a*,*b*), λ is a similarity parameter defined to take the value $\lambda=0$ at the plate trailing edge (point of separation), i.e.

$$Z(0)=0, \tag{4.2}$$

while $\lambda=1$ corresponds to the vortex-sheet free edge. The circulation, Γ, is constant at any material point on the vortex sheet; see § 3.1. Defining $\Gamma_0(T)=\Gamma$ at the plate trailing edge ($\lambda=0$), from (4.1*a*,*b*) it then follows that the total shed circulation is

$$\Gamma_0(T)=U_0 a\mathcal{J}T^s, \tag{4.3}$$

where $\mathcal{J}$ is henceforth termed the 'shed circulation constant'.

Substitution of (4.1*a*,*b*) into (3.3) and (3.4) and utilizing (2.13) and (2.10*a*,*b*) gives, after some algebra

$$\begin{aligned}T^{q-1}\left(q\bar{Z}+s(1-\lambda)\frac{d\bar{Z}}{d\lambda}\right)&=T^m\cos\left(\alpha_0+\frac{\beta}{1+p}T^{1+p}\right)\\&\quad-\frac{\mathrm{i}}{Z^{1/2}}\left(\frac{1}{2^{1/2}}T^{-q/2}\tilde{Q}(T)+\frac{\mathcal{J}}{4\pi}T^{s-q}I(Z)\right),\end{aligned} \tag{4.4}$$

where

$$I(Z)=\int_0^1\left(\frac{1}{Z^{1/2}-Z'^{1/2}}-\frac{1}{Z^{1/2}+\overline{Z}'^{1/2}}\right)\mathrm{d}\lambda', \tag{4.5a}$$

$$\tilde{Q}(T)=T^p\beta\left(\frac{1}{2}-d\right)+T^m\sin\left(\alpha_0+\frac{\beta}{1+p}T^{1+p}\right), \tag{4.5b}$$

and the Kutta condition becomes

$$\frac{\mathcal{J}}{4\pi}T^{s-q/2}\int_0^1\left(\frac{1}{Z^{1/2}}+\frac{1}{\bar{Z}^{1/2}}\right)\mathrm{d}\lambda=\frac{1}{2^{1/2}}\tilde{Q}(T),\tag{4.6}$$

where $Z'\equiv Z(\lambda')$. The left-hand side of (4.4) is the time derivative on the left-hand side of (3.3). The first term on the right-hand side is the convective free stream, while the two terms in brackets on the right-hand side are respectively the singular attached flow and the vortex-sheet induced velocity.

Equation (4.4) forms the basis of our analysis of the starting vortex. The control parameters are $(m, p, \alpha_0, d, \beta)$ which are to be specified; see start of § 3 for their physical meaning.

4.2. *Dominant-balance analysis*

As discussed in § 1, our focus is on the primitive start-up vortex. We thus consider the limit of small convective time, T, when performing a dominant-balance analysis of (4.4)–(4.6). In seeking a time-dependent solution, the unsteady term on the left-hand side of (4.4) must be retained because it represents the highest-order time derivative in the system. We now search for dominant terms on the right-hand side that will balance the unsteady term in powers of T in the limit $T\to 0^+$. Owing both to the structure of $\tilde{Q}(T)$ in (4.5*b*) which contains two terms, and also the trigonometric functions of $\alpha(T)$ in (4.4) and (4.5*b*), which also have two terms, different scenarios must be considered.

The parameter space can be explored with four distinct plate motions: (*a*) $\alpha_0=0$ with (i) $d\neq 1/2$ and (ii) $d=1/2$; (*b*) $\alpha_0\neq 0$ with (i) $d\neq 1/2$ and (ii) $d=1/2$. Starting flows with $d=1/2$ (rotation about the three-quarter chord point) may differ from those with $d\neq 1/2$ because for the former, the coefficient of β in (4.5*b*) is zero. Likewise flows with non-zero initial angle of attack, i.e. $\alpha_0\neq 0$, will have different start-up behaviour from those with $\alpha_0=0$. The latter will be seen to be delicate because the trailing-edge singularity can take a weak form. In the following, we consider these four classes by obtaining the relevant power-law growth of both the starting-vortex trajectory and circulation.

In the next section, a detailed solution of the flow generated by the first distinct plate motion, $\alpha_0=0$ with $d\neq 1/2$, corresponding to zero initial angle of attack and rotation away from the plate three-quarter chord position, respectively, is developed together with sample numerical solutions; see § 5.1. For brevity, cursory analyses of the other three distinct plate motions are presented in §§ 5.2–5.4 with details and numerical case studies left to the reader.

5. Four distinct plate motions

5.1. $\alpha_0=0,\ d\neq 1/2$

This first distinct plate motion produces the most novel starting-vortex dynamics and is documented in detail in this section. Here, the second term in $\tilde{Q}(T)$ in (4.5*b*), of order T^{1+m+p}, can always be neglected compared to the first term. Further, we can take $\cos(\alpha(t))=1+O(T^{2(1+p)})=1$ to the order required. To leading order, the Kutta condition (4.6) is then

$$\frac{\mathcal{J}}{4\pi}T^{s-q/2}\int_0^1\left(\frac{1}{Z^{1/2}}+\frac{1}{\bar{Z}^{1/2}}\right)\mathrm{d}\lambda=\frac{1}{2^{1/2}}T^p\hat{\beta},\tag{5.1}$$

where the following composite parameter naturally emerges,

$$\hat{\beta} = \beta\left(\tfrac{1}{2} - d\right). \tag{5.2}$$

For finite shed circulation, (5.1) requires

$$s = q/2 + p. \tag{5.3}$$

The parameter p, defined in (2.10*a*,*b*), is a key control parameter specifying rotational motion of the plate, whereas q and s describe the vortex motion and are to be determined. Equation (4.4) therefore becomes

$$T^{q-1}\left(q\bar{Z} + (q/2+p)(1-\lambda)\frac{\mathrm{d}\bar{Z}}{\mathrm{d}\lambda}\right) = T^{m} - T^{-q/2+p}\frac{\mathrm{i}}{Z^{1/2}}\left(\frac{1}{2^{1/2}}\hat{\beta} + \frac{\mathcal{J}}{4\pi}I(Z)\right). \tag{5.4}$$

We consider three separate cases for the primitive start-up vortex, i.e. for $T \ll 1$, which we denote Type I, Type II and Type III, respectively.

5.1.1. *Type I vortex sheet*

We first examine when rotational motion of the plate dominates convection due to its translation. For kinematic reasons, we expect the vortex-sheet roll-up centre to be shed (approximately) normal to the plate's trailing edge. This corresponds to a dominant balance between the left-hand side and the second term on the right-hand-side of (5.4). Equating powers of T and using (5.3) gives $q = 2(1+p)/3$ and $s = (4p+1)/3$. For the first term on the right-hand side of (5.4) to remain subdominant, we require $m > q - 1$, i.e. $m > (2p-1)/3$. Substituting these results into (4.1*a*,*b*) and (4.3) provides the required solution,

$$\frac{\hat{z}_v}{a} = T^{2(1+p)/3}Z(\lambda), \quad \tilde{\Gamma} \equiv \frac{\Gamma_0(T)}{U_0 a} = \mathcal{J}T^{(1+4p)/3}, \quad \text{for } m > \frac{2p-1}{3}, \tag{5.5a,b}$$

where $Z(\lambda)$ and the shed circulation constant, $\mathcal{J}$, are now determined by the integro-differential equation (IDE) obtained by retaining the dominant terms in (5.4),

$$\frac{2}{3}(1+p)\left(\bar{Z} + \frac{4p+1}{2(p+1)}(1-\lambda)\frac{\mathrm{d}\bar{Z}}{\mathrm{d}\lambda}\right) = -\frac{\mathrm{i}}{Z^{1/2}}\left(\frac{1}{2^{1/2}}\hat{\beta} + \frac{\mathcal{J}}{4\pi}I(Z)\right), \tag{5.6}$$

subject to the initial condition, (4.2), and the Kutta condition

$$\mathcal{J}\int_0^1 \left(\frac{1}{Z^{1/2}} + \frac{1}{\bar{Z}^{1/2}}\right)\mathrm{d}\lambda = 2\sqrt{2}\pi\hat{\beta}. \tag{5.7}$$

The change of variables

$$\mathcal{J} = AJ, \quad Z = B\omega, \tag{5.8a,b}$$

where

$$A = \left(\frac{3\hat{\beta}^4}{1+p}\right)^{1/3}, \quad B = \frac{1}{2}\left(\frac{3\hat{\beta}}{1+p}\right)^{2/3}, \tag{5.9a,b}$$

maps (5.6) and (5.7) into (35) and (36) of Pullin (1978) (with $n = 1/2$), reproduced here as

$$\bar{\omega} + \frac{4p+1}{2(p+1)}(1-\lambda)\frac{\mathrm{d}\bar{\omega}}{\mathrm{d}\lambda} = -\frac{\mathrm{i}}{\omega^{1/2}}\left(1 + \frac{J}{2\pi}I(\omega)\right), \tag{5.10}$$

with $\omega(0) = 0$ (see (4.2) and (5.8*a*,*b*)) and the Kutta condition is

$$\frac{J}{2\pi}\int_0^1 \left(\frac{1}{\omega^{1/2}} + \frac{1}{\bar{\omega}^{1/2}}\right)\mathrm{d}\lambda = 1, \tag{5.11}$$

which eliminates the composite parameter, $\hat{\beta}$.

5.1.2. *Numerical method*

Numerical solutions displayed in figure 9(*a*) of Pullin (1978) show the starting-vortex shape in the ω variable corresponding to Type I starting vortices. The solution for impulsive start up was later independently verified by Jones (2003). Solutions are re-calculated here using the numerical method of Pullin (1978), for which we now provide a brief summary. The vortex sheet is divided into two parts. The first is a continuous section in $0 \le \lambda \le \lambda_N$ represented by N straight segments with the first segment joined to the plate trailing edge. The second is an inner section modelled by a point vortex of strength, $J(1-\lambda_N)$, located at $\omega = \omega_{N+1}$ that is joined to the end of the continuous section by a cut in the ω-plane from $\omega(\lambda_N)$ to ω_{N+1}. A finite-difference form of the IDE in (5.10) is satisfied at the midpoint of each segment of the continuous sheet using a two-point rule for derivatives and a trapezoidal rule for the Cauchy principal value integrals, giving $2N$ equations. This involves some error owing to neglected logarithmic corrections arising from proximity of a point on the sheet to nearby segments on adjacent spiral turns. This, however, is mitigated by cancellation because most points lie inside a tightly wound spiral with many individual turns on either side. On the inner portion, point-wise solution of the IDE is replaced by implementing an integrated form of the IDE over $\lambda_N \le \lambda \le 1$, providing two further equations. This is equivalent to requiring zero total force on the cut-isolated vortex system (Rott 1956). A similar representation of the Kutta condition is used leading a total of $2(N+1)+1$ equations.

The discrete implementation does not fix a discrete set, λ_i $(i = 1, \ldots, N)$, and then solve for ω_j $(j = 1, \ldots, 2(N+1))$ and J. Instead, on the inner portion of the sheet, a transformation to polar coordinates centred on ω_{N+1} is utilized. With fixed polar angles for points on the sheet (relative to this chosen but unknown centre), the $2(N+1)+1$ unknowns become a set of radii $|\omega_{N+1} - \omega_j|$ and λ_j, $j = 1, \ldots, N$, ω_{N+1} and J. This method enhances robustness because the number of discrete points per sheet turn can then be easily controlled. The set of $2(N+1)+1$ nonlinear equations are solved with a Newton–Raphson method. The numerical method is implemented in Fortran, as originally coded for Pullin (1978) (personal hard copy (1978), modified for the present work).

Numerical solutions are given in figure 4 for three cases: constant impulsive angular speed, $p = 0$, linearly increasing angular speed, $p = 1$, and the asymptotic angular speed limit, $p \to \infty$. These are obtained with $N = 2400$ points on the vortex sheet and each contain about 33 individual sheet turns (around the vortex core) with approximately 70–80 points on each turn. The inner portion of the rolled-up sheet is asymptotic to a tightly wound algebraic spiral whose structure, including the spacing between turns, depends on the plate rotational control parameter, p (Kaden 1931; Pullin 1978). The choice of 33 sheet windings is more than sufficient for numerical solutions to reach this asymptotic form; see figure 5 and (22) of Pullin (1978). In the sheet shape depictions, we show a

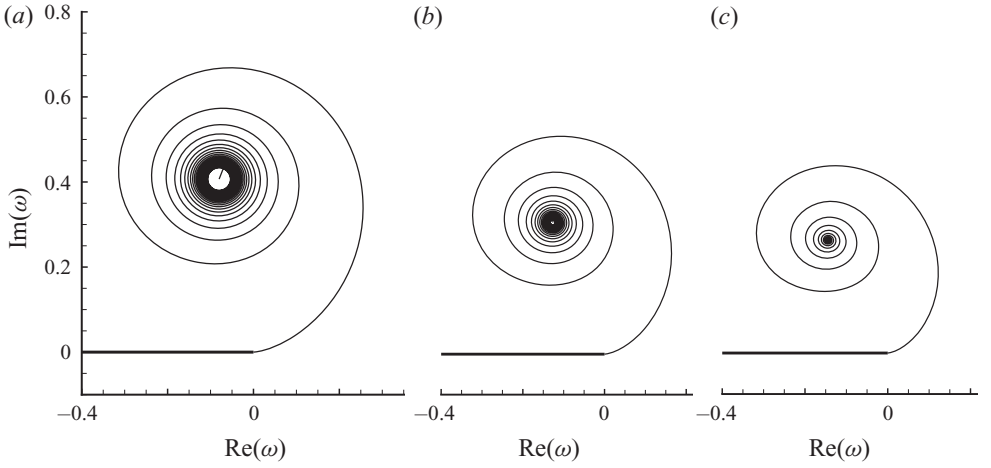

FIGURE 4. Examples of Type I vortex-sheet solutions. These are a family with parameter, p. Solutions are given for (*a*) $p = 0$, (*b*) $p = 1$, (*c*) $p \to \infty$. For the plate motion described in § 5.1, this solution gives the sheet shape corresponding to zero initial angle of attack, $\alpha_0 = 0$, pivot point away from the three-quarter chord position, $d \neq 1/2$, and plate rotation dominating its translation, $m > (2p - 1)/3$, where m and p are the plate translation and rotation power laws, respectively. Results shown in the ω-plane, which is a uniformly scaled version of the Z-plane; see (5.5*a*,*b*) and (5.8*a*,*b*).

straight line joining the end of the continuous part of the sheet to the central point vortex located at ω_{N+1}, which is taken as the centre of roll up. This can be seen in figure 4(*a*) for $p = 0$. The branch cut starts at the point vortex, runs along this line to the free end of the vortex sheet, then along the spiral sheet to the plate trailing edge and finally along the plate to its leading edge. In figure 4(*a*), $\lambda_{2400} = 0.8936$ meaning that the (curved) vortex sheet carries 89 % of the total circulation, while the central point vortex carries the remaining 11 %. For $p = 1$ in figure 4(*b*), $1 - \lambda_{2400} = 0.0077$ so that the central point vortex carries less than 1 % of the total shed circulation. Figure 4(*c*) gives results for $p \to \infty$ with $1 - \lambda_{2400} = 1.4319 \times 10^{-8}$; for comparison, $1 - \lambda_{2399} = 1.4397 \times 10^{-8}$ illustrating the convergence with N. Details of numerical convergence with respect to both mesh refinement along the sheet and the number of spiral turns are given in the Appendix.

For the present case, plate rotation is dominant over its translation. Indeed, our finding that (5.10) and (5.11) are independent of the composite parameter, $\hat{\beta}$, is consistent with this restriction, i.e. the geometrical structure of Type I vortex sheets do not depend on the relative strength of plate rotation-to-translation speeds; they are also independent of the rotational position, d.

We emphasize that Type I vortex sheets are a one-parameter family of curves and J values that depend on the rotational power law, p. In addition to $\alpha_0 = 0$ studied here, it will be seen in §§ 5.3 and 5.4 that these Type I vortex-sheet solutions describe all possible starting vortices for non-zero angle of attack, $0 < \alpha_0 < \pi/2$, with one exception (discussed end of § 5.3).

5.1.3. *Type II vortex sheet*

Next, we study when translational convection dominates rotational motion of the plate. This corresponds to a dominant-balance analysis between the left-hand side and the first term on the right-hand side of (5.4). Equating powers of T in these terms then gives

$q = 1 + m$ and hence $s = p + (m + 1)/2$ via (5.3). A sub-dominant second term on the right-hand side of (5.4) requires $m < -q/2 + p$ which is equivalent to $m < (2p - 1)/3$. Hence,

$$\frac{\hat{z}_v}{a} = T^{1+m} Z(\lambda), \quad \tilde{\Gamma} \equiv \frac{\Gamma_0(T)}{U_0 a} = \mathcal{J} T^{p+((1+m)/2)}, \quad \text{for } m < \frac{2p-1}{3}, \tag{5.12a,b}$$

where $Z(\lambda)$ is determined by solution to the linear differential equation,

$$(1+m)Z + \left(p + \frac{1+m}{2}\right)(1-\lambda)\frac{\mathrm{d}Z}{\mathrm{d}\lambda} = 1, \tag{5.13}$$

subject to the initial condition in (4.2). Here, owing to the subdominant vortex-induction term in (5.4), the Kutta condition (5.1) decouples from (5.13) and can be expressed as

$$\mathcal{J} = \sqrt{2}\pi\hat{\beta}\left(\int_0^1 Z^{-(1/2)}\,\mathrm{d}\lambda\right)^{-1}. \tag{5.14}$$

Equations (5.13) and (5.14) have the exact solution

$$Z(\lambda) = \frac{1}{1+m}\left(1 - (1-\lambda)^b\right), \tag{5.15a}$$

$$\mathcal{J} = \hat{\beta}\sqrt{\frac{2\pi}{1+m}}\,\frac{\Gamma_c\left(1 + \dfrac{p}{1+m}\right)}{\Gamma_c\left(\dfrac{3}{2} + \dfrac{p}{1+m}\right)}, \tag{5.15b}$$

where

$$b = \frac{2(1+m)}{1+m+2p}, \tag{5.16}$$

and Γ_c is the complete gamma function (not to be confused with the circulation Γ_0). The solution for $Z(\lambda)$ in (5.15*a*) lies on the real axis and thus corresponds to a vortex sheet that is strictly parallel to plate (even as it rotates). We now explore how this vortex-sheet rigid body rotation arises.

Importantly, there is a weak singularity in the attached flow at the plate trailing edge which must be cancelled by finite shed circulation. Since the effect of the shed circulation and its image is still felt by the separated flow, this leads to rigid body rotation of the vortex sheet in concert with that of the plate. The overall result is that the vortex-sheet shape growth (5.15*a*) does not depend on the rotation parameter, $\hat{\beta}$, but the shed circulation retains dependence to order $\hat{\beta}$. The separation is convection dominated but (rigid body) rotational effects remain. The solution includes the limiting case of vanishing initial angle of attack, $\alpha(t) \to 0$, and plate rotation, $\hat{\beta} \to 0$, where the plate slices through the fluid parallel to its plane with zero shed circulation. The vortex sheet still forms and moves with the same speed, but its circulation is $O(\hat{\beta})$, and thus vanishingly small as $\hat{\beta} \to 0$.

A (dimensional) circulation centroid can be calculated,

$$\langle \hat{x} \rangle = aT^{1+m} \int_0^1 Z(\lambda)\, \mathrm{d}\lambda = aT^{1+m} \frac{3}{3+3m+2p}, \tag{5.17}$$

while the (dimensional) velocity jump at the trailing edge is

$$\gamma = U_0 \mathcal{J} \left(p + \frac{1+m}{2} \right) T^{p-((1+m)/2)}, \tag{5.18}$$

and is finite.

Type II vortex sheets are similar but not identical to point-vortex solutions obtained by Tchieu & Leonard (2011) who use an impulse-conserving formulation. Importantly, Type II solutions exist only for zero angle of attack, $\alpha_0 = 0$ (the case studied here), with one exception discussed in the last paragraph of § 5.3.

5.1.4. *Type III vortex sheet*

The form of Type I and Type II vortex-sheet solutions above shows that, for fixed and finite $\hat{\beta}$, the solution changes discontinuously and remarkably as a state point in the (m, p) plane crosses the line, $m = (2p-1)/3$:

(*a*) Type I ($m > (2p-1)/3$): a vortex-induction dominated, separated, spiral sheet exists, whose line joining the centre of roll-up to the plate trailing edge makes an angle with the positive x axis greater than $\pi/2$, i.e. the vortex core sits over the plate.

(*b*) Type II ($m < (2p-1)/3$): a flat vortex sheet arises that separates parallel to the plate that undergoes rigid body rotation with the plate.

On the line, $m = (2p-1)/3$, a third class of vortex sheet exists that forms an intermediate vortex-state transition (VST) between Types I and II. This is referred to as a Type III vortex sheet. With $m = (2p-1)/3$, all terms in (5.4) then have the same power exponent of T and balance, i.e. the contributions of translational convection and rotational motion of the plate balance precisely. The governing equation for Type III is nearly identical to (5.6), except it contains an extra term equal to unity on the right-hand side. Again using the change of variables in (5.8*a*,*b*), (5.4) becomes

$$\bar{\omega} + \frac{4p+1}{2(p+1)}(1-\lambda)\frac{\mathrm{d}\bar{\omega}}{\mathrm{d}\lambda} = \left(\frac{(1+p)\hat{\beta}^2}{3} \right)^{-(1/3)} - \frac{\mathrm{i}}{\omega^{1/2}} \left(1 + \frac{J}{2\pi} I(\omega) \right), \tag{5.19}$$

while the Kutta condition (5.1) remains identical to (5.11). Here, the composite parameter, $\hat{\beta}$, cannot be scaled out, and so solutions will depend on its value. We therefore immediately see that the flow at this singular condition, $m = (2p-1)/3$, where convection and rotation balance, produces novel separation-flow physics.

Numerical solutions to (5.11) and (5.19) are given in figures 5–7, for the example case of impulsive and constant translational plate speed, $m = 0$, and a time varying angular speed with $p = 1/2$. The numerical method described previously for Type I solutions is used, where a vortex discretization of $N = 1,220$ is found to be sufficient for convergence (see the Appendix). Vortex sheets displayed in figures 5–7 have 15 turns on the continuous sheet, which again is sufficient to capture the Kaden, inner asymptotic form. We show the properties of solutions in both the (stretched) ω and (unscaled) Z planes. Although these

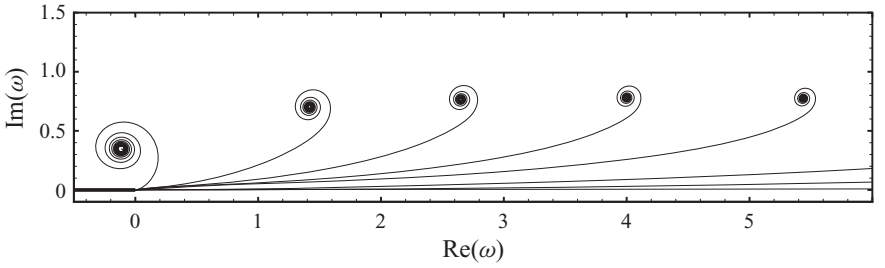

FIGURE 5. Type III vortex sheets (plate rotation balancing its translation) for zero initial angle of attack, $\alpha_0 = 0$, impulsive and constant translational plate speed, $m = 0$, pivot point away from the three-quarter chord position, $d \neq 1/2$, with angular speed power law, $p = 1/2$. Vortex sheets with visible cores (left to right): $\hat{\beta} \to \infty$ and $\hat{\beta} = 1,\ 0.5,\ 0.3,\ 0.2$. Vortex sheets with cores not visible at $\mathrm{Re}\{\omega\} = 6$ (top to bottom): $\hat{\beta} = 0.1,\ 0.05,\ 0.01$. Results shown in the ω-plane.

are simply rescaled versions of each other, we show both because – owing to their respective divergences – the limiting solution for $\hat{\beta} \to \infty$ cannot be depicted using the $Z(\lambda)$-description, while the solution for $\hat{\beta} \to 0$ cannot be shown graphically using the $\omega(\lambda)$ function.

In figure 5, the vortex-sheet profiles are plotted in the ω-plane for $\hat{\beta} \to \infty$ and $\hat{\beta} = 1,\ 0.5,\ 0.3,\ 0.2$. The limit, $\hat{\beta} \to \infty$, corresponds to a Type I solution, i.e. the plate rotational motion dominates translational convection. As $\hat{\beta}$ decreases, the vortex core moves downstream while becoming more compact. When $\hat{\beta} \to 0$, the vortex core moves further downstream and approaches infinity on the real ω axis, with distance increasing as $\hat{\beta}^{-2/3}$. This scaling relation follows from (5.8*a*,*b*), together with the result (to be shown subsequently in this subsection), that at the vortex-sheet free edge ($\lambda = 1$), $Z \to 1 + 0i$ as $\hat{\beta} \to 0$. This shows the transition from rotation-dominated to convection-dominated separation. It can also be observed in figure 5, that the height of the vortex centre appears almost constant (occurring at $\mathrm{Im}\{\omega\} \approx 0.75$) for solutions with $\hat{\beta} = 0.5,\ 0.3,\ 0.2$. As $\hat{\beta}$ decreases further, however, numerical solutions (not displayed) do show a weak but definite decrease in this height (in the ω-plane), e.g. the centre of roll up when $\hat{\beta} = 0.001$ occurs at $\omega = 199.93 + 0.3240i$.

Figure 6(*a*) shows vortex-sheet profiles in the Z-plane while figure 6(*b*) focuses on behaviour near the plate trailing edge for very small $\hat{\beta}$. In the Z-plane, the vortex-sheet extent become infinitely large as $\hat{\beta} \to \infty$. As $\hat{\beta}$ decreases, the sheet contracts in extent while the size of the rolled-up core reduces in size in comparison with the distance of the roll-up centre from the trailing edge. When $\hat{\beta} \to 0$, the centre approaches $Z = 1 + 0i$ which, from (5.15*a*), corresponds to the flat sheet edge for a Type II vortex sheet with $m = 0$. For all finite $\hat{\beta}$, there exists a tightly wound spiral section containing an infinite number of sheet turns. This is where vortex self-induction remains locally dominant over convection. Figure 7 shows two close-up portraits of the vortex-sheet profile in the Z-plane for $\hat{\beta} = 1$ and 0.001. The general structure is similar. At the centre of roll up, both have the form of a Kaden spiral with small elliptical corrections of the type discussed by Moore (1975) and Guiraud & Zeytounian (1977).

Approach of Type III to the limiting Type II vortex sheet is illustrated in figure 8. This shows Cartesian coordinates of the vortex sheets, $X(\lambda) = \mathrm{Re}\{Z(\lambda)\}$ and $Y(\lambda) = \mathrm{Im}\{Z(\lambda)\}$,

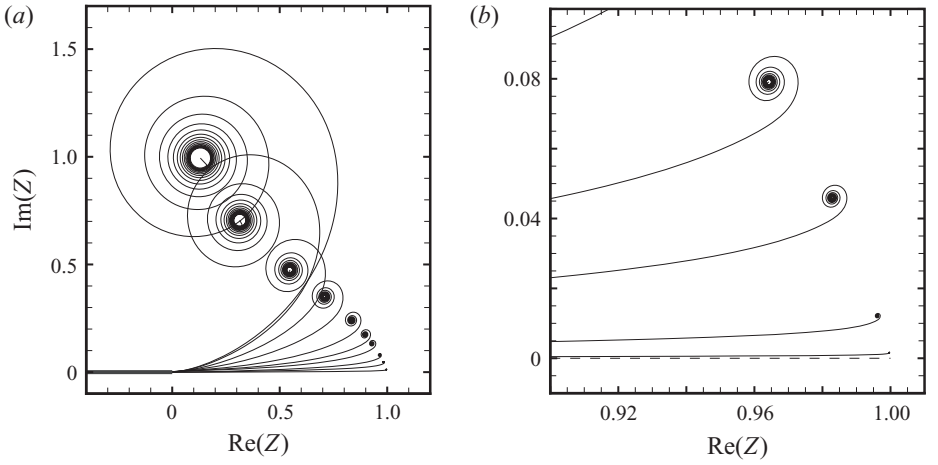

FIGURE 6. Type III vortex sheets, as for figure 5, but now including smaller values of $\hat{\beta}$ and shown in the Z-plane. (*a*) Top left to bottom right: $\hat{\beta} = 10, 5, 2, 1, 0.5, 0.3, 0.2, 0.1, 0.05, 0.01$. (*b*) $\hat{\beta} = 0.1, 0.05, 0.01, 0.001$, with dashed horizontal line provided for reference only.

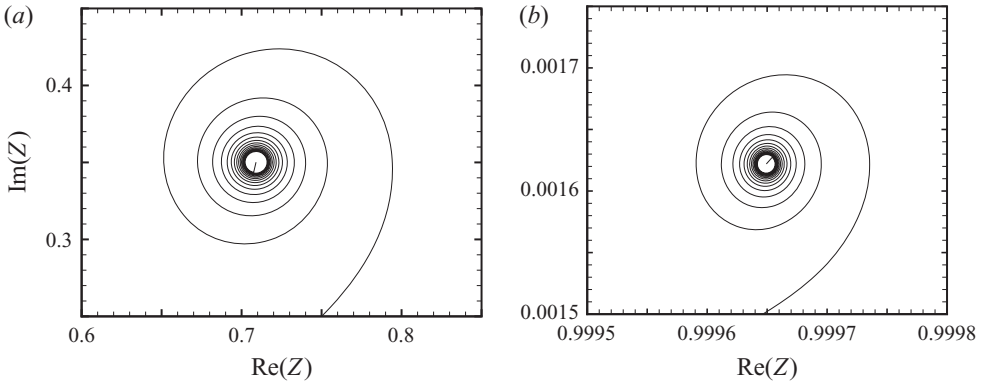

FIGURE 7. Close ups of Type III vortex sheets in figure 6, for (*a*) $\hat{\beta} = 1$, (*b*) $\hat{\beta} = 0.001$. For comparison, the vortex sheets are plotted on identical square domains of size, $0.3\hat{\beta} \times 0.3\hat{\beta}$.

where $\lambda = 0$ and 1 coincide with the plate trailing edge and vortex-sheet free edge, respectively, as function of $\hat{\beta}$. From (5.15*a*), the Type II solution is simply, $Z = \lambda$, i.e. a horizontal line of finite length, for the plate control parameters studied in figures 5 and 6, i.e. $m = 0$ and $p = 1/2$. Approach of the Type III vortex sheet to the limiting Type II sheet, as $\hat{\beta} \to 0$, is clear in figure 8: $X(\lambda)$ asymptotes to the required straight line of slope one and $Y(\lambda)$ approaches zero. Notably, for any small and non-zero $\hat{\beta}$, there exists a small region near $\lambda = 1$ where rapid and decaying oscillations occur. This corresponds to roll-up near the vortex-sheet free edge, which approaches this free edge and vanishes in the limit of small $\hat{\beta}$. The small straight lines that can be seen in figure 8 near $\lambda = 1$ represent the inner portion of the numerical sheet model, where its end is joined to the central point vortex.

Finally, we study the shed circulation constant, $\mathcal{J}$, defined in (4.3). For a Type II vortex sheet, with the example control parameters, $m = 0$ and $p = 1/2$, used in this section,

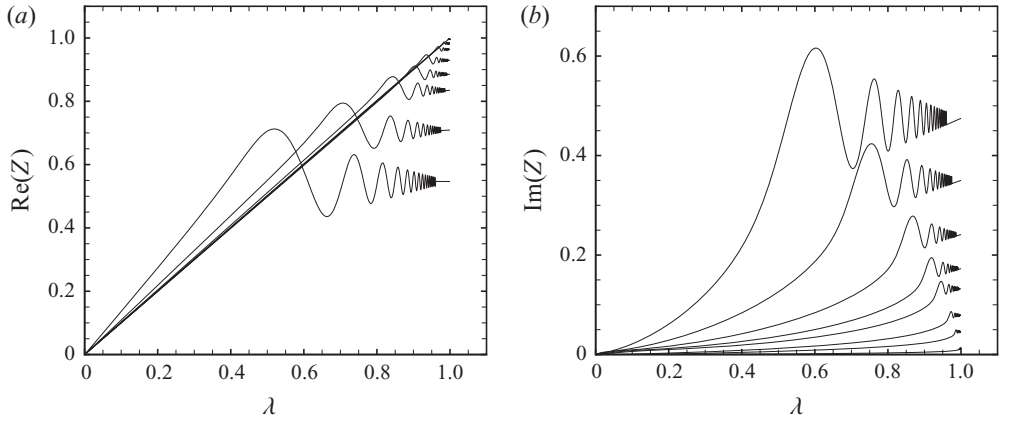

FIGURE 8. Type III vortex sheets, as for figure 5, showing their Cartesian coordinates for $\hat{\beta} = 2, 1, 0.5, 0.3, 0.2, 0.1, 0.05, 0.01$. (*a*) $X(\lambda) = \mathrm{Re}\{Z(\lambda)\}$ with $\hat{\beta}$ decreasing bottom to top, (*b*) $Y(\lambda) = \mathrm{Im}\{Z(\lambda)\}$ with $\hat{\beta}$ decreasing top to bottom. Limiting Type II solution: $Z(\lambda) = \lambda + 0i$.

(5.15*b*) gives

$$\left.\frac{\mathcal{J}}{\hat{\beta}}\right|_{Type\ II} = \sqrt{\frac{\pi}{2}}\frac{\Gamma_c\left(\frac{3}{2}\right)}{\Gamma_c(2)} = \frac{\pi}{2\sqrt{2}} \approx 1.11072. \tag{5.20}$$

In contrast, the dependence of $\mathcal{J}$ on $\hat{\beta}$ for a Type III vortex sheet follows from (5.8*a*,*b*) and (5.9*a*,*b*),

$$\left.\frac{\mathcal{J}}{\hat{\beta}}\right|_{Type\ III} = \frac{1}{2}\hat{\beta}^{1/3}J(\hat{\beta}), \tag{5.21}$$

where $J(\hat{\beta})$ is determined numerically. Figure 9 gives numerical results for the Type II solution in (5.21); the Type III formula, (5.20), is the dashed horizontal line. Again the approach of the Type III formula to the limiting Type II solution as $\hat{\beta} \to 0$ is clear. For $\hat{\beta} \to \infty$, $J(\hat{\beta}) \to 2.3551$ and so from (5.21) we obtain

$$\left.\frac{\mathcal{J}}{\hat{\beta}}\right|_{Type\ III} \approx 1.178\hat{\beta}^{1/3}, \quad \hat{\beta} \gg 1, \tag{5.22}$$

which is shown as the dash-dot line in figure 9.

5.1.5. *Special case: impulsive and constant translational plate speed*

We consider the special case where the plate translates impulsively at constant speed, i.e. $m = 0$, and examine the vortex transitions as the plate rotational power-law, p, is varied. For a fixed relative strength of plate rotation to translation, β (and hence $\hat{\beta}$), and a rotational power law in the range, $0 \le p < 1/2$, the starting vortex is always of Type I. The numerical solutions in the ω-plane for Type I vortices in figure 4 are independent of m and $\hat{\beta}$, by definition, and thus applicable here. These show that the line joining the vortex centre to the plate trailing edge is approximately normal to the plate, at an angle to the plate that decreases slightly with increasing p. The vortex position above the plate and its circulation grow with power laws of the dimensionless time equal to $2(1 + p)/3$ and

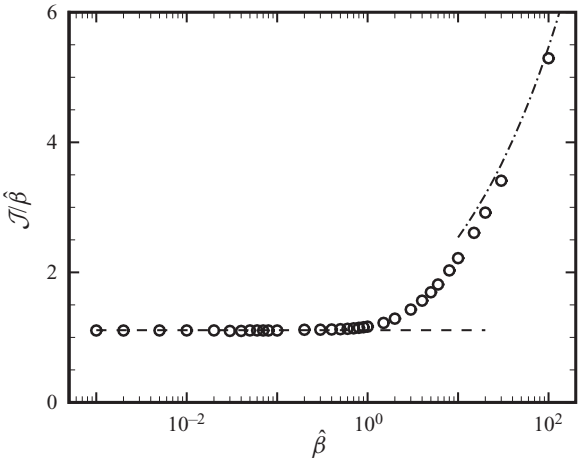

FIGURE 9. Shed circulation constant, $\mathcal{J}$, as a function of $\hat{\beta}$ for a Type III vortex sheet, with plate control parameters as specified in figure 5. Dots obtained using (5.21) for Type III vortex sheet are valid for all $\hat{\beta}$. Type III high $\hat{\beta}$ solution is dot-dashed line. For comparison, Type II solution in (5.20) is horizontal dashed line.

$(1 + 4p)/3$, respectively. As $p \to 1/2^-$, these Type I power laws both approach unity, i.e. linear growth in time occurs.

The change from $p \to 1/2^-$ to $p = 1/2$ provides a discontinuous transition to a new state for which the $Z(\lambda)$ profiles are of Type III as shown in figure 6, for two particular values of $\hat{\beta}$. For $p = 1/2$, both the vortex position and circulation growth remain proportional to time, but the vortex shedding angle (to the plate) increases with $\hat{\beta}$, i.e. the vortex moves downstream. A further discontinuous transition occurs from $p = 1/2$ to $p \to 1/2^+$. The vortex trajectory is then of Type II, i.e. parallel to and downstream of the plate, and remains so for $p > 1/2$. Its flat $Z(\lambda)$ profile is independent of $\hat{\beta}$ in contrast to its circulation. The circulation grows with a time power law of $p + 1/2$. This behaviour is close, but not identical to that predicted by Tchieu & Leonard (2011). Moreover, in the present model this transition occurs only for $\alpha_0 = 0$, i.e. zero initial angle of attack.

Consequently, the vortex trajectory and circulation growth are both twice discontinuous as p passes through $p = 1/2$ with $\hat{\beta}$ fixed. This vortex-state change Type I $\to$ Type III $\to$ Type II with increasing p, appears to be a consequence of the change in strength of the weak attached-flow singularity at the trailing edge. We give numerical results in § 6 that may form the basis for future high Reynolds number viscous flows designed to test for the existence of this vortex-state transition.

5.1.6. *General case: accelerating translational plate motion*

Finally in this section, we study the general case where the plate translational speed varies with time, i.e. $m \geq 0$; this includes constant translational speed explored in § 5.1.5. For a Type I vortex sheet, the ratio of the (neglected) convective term to the vortex-induction term in (5.4), i.e. the first and second terms on the right-hand side of (5.4), respectively, is $R \sim T^{m-(2p-1)/3}$. Suppose $p = (1 + 3m)/3 - 3\epsilon/2$ where $0 < \epsilon \ll 1$, i.e. near the VST point where the first and second right-hand side terms of (5.4) balance, then $R \sim T^{\epsilon}$. Now let $T = 10^{-c}$ where $c > 0$, giving $R \sim 10^{-c\epsilon}$. Dominance of vortex self-induction over convection in a Type I vortex sheet, i.e. $R \ll 1$, then requires $c \gg \epsilon^{-1}$.

Hence, as the VST point is approached, i.e. $\epsilon \to 0$, we find $c \to \infty$, leading to $T \to 0$. That is, a Type I vortex sheet can be uniquely distinguished only over a vanishingly small start-up flow time. Nonetheless, this also shows that for any small but finite ϵ, i.e. a 'finite distance' from the VST point, there exists a sufficiently small start-up time window where a Type I vortex sheet will be observable. Similar arguments can be constructed for the transition from a Type II to III vortex sheet, by choosing $p = (1 + 3m)/3 + 3\epsilon/2$ for finite $\hat{\beta}$.

Next, we turn our attention to the three remaining distinct plate motions, but study them in less detail than provided in the present section for $\alpha_0 = 0$, $d \neq 1/2$.

5.2. $\alpha_0 = 0$, $d = 1/2$

This corresponds to a plate with zero initial angle of attack, $\alpha_0 = 0$, that is rotating about its three-quarter chord point, $d = 1/2$. Here, the term in (4.4) that drives circulation growth becomes, $\tilde{Q}(T) = \beta(1 + p)^{-1}T^{1+m+p}$, plus higher-order terms in the limit of small T (see (4.5*b*)), and we similarly expand $\cos(\alpha(t)) = 1 + O(T^{2(1+p)}) = 1$, to the order required. Balancing the Kutta condition, (4.6), then gives

$$s = \frac{q}{2} + m + p + 1, \tag{5.23}$$

and (4.6) becomes

$$\frac{\mathcal{J}}{4\pi}\int_0^1 \left(\frac{1}{Z^{1/2}} + \frac{1}{\bar{Z}^{1/2}}\right) \mathrm{d}\lambda = \frac{1}{2^{1/2}}\frac{\beta}{1+p}. \tag{5.24}$$

Substituting (5.23) into (4.4) gives

$$\begin{aligned} &T^{q-1}\left(q\bar{Z} + \left[\frac{q}{2} + 1 + m + p\right](1-\lambda)\frac{\mathrm{d}\bar{Z}}{\mathrm{d}\lambda}\right) \\ &\quad = T^m - T^{-(q/2)+1+m+p}\frac{\mathrm{i}}{Z^{1/2}}\left(\frac{1}{2^{1/2}}\frac{\beta}{1+p} + \frac{\mathcal{J}}{4\pi}I(Z)\right). \end{aligned} \tag{5.25}$$

Again, there are three flow types. The first arises from a dominant balance between the left-hand side and the second term on the right-hand side of (5.25), i.e. a plate rotation-dominated flow. This gives $q = 2(2 + m + p)/3$ and $s = (5 + 4m + 4p)/3$ with

$$\frac{\hat{z}_v}{a} = T^{(2/3)(2+m+p)}Z(\lambda), \quad \tilde{\Gamma} = \mathcal{J}T^{(1/3)(5+4m+4p)}, \quad \text{for } m > 1 + 2p, \tag{5.26a,b}$$

where $Z(\lambda)$ and the shed circulation constant, $\mathcal{J}$, are determined from the solution of an integro-differential equation similar to (5.1) and (5.6).

A plate translation-dominated flow is obtained by performing a dominant balance between the left-hand side and the first term on the right-hand side of (5.25), giving $q = 1 + m$ and $s = 3(1 + m)/2 + p$, with

$$\frac{\hat{z}_v}{a} = T^{1+m}Z(\lambda), \quad \tilde{\Gamma} = \mathcal{J}T^{(3/2)(1+m)+p}, \quad \text{for } m < 1 + 2p, \tag{5.27a,b}$$

where $Z(\lambda)$ and $\mathcal{J}$ are obtained from solution of a linear system similar to (5.13) and (5.14), giving a Type II vortex sheet. The balance, $m = 1 + 2p$, gives a Type III vortex sheet similar to that described earlier but with different power laws and constants; details are left to the reader.

5.3. $\alpha_0 \neq 0$, $d \neq 1/2$

We now consider a plate with non-zero initial angle of attack, $\alpha_0 \neq 0$, that is rotating away from its three-quarter chord point, $d \neq 1/2$. The Kutta condition, (4.6), to leading order in T is

$$\frac{\mathcal{J}}{4\pi} T^{s-(q/2)} \int_0^1 \left(\frac{1}{Z^{1/2}} + \frac{1}{\bar{Z}^{1/2}} \right) \mathrm{d}\lambda = \frac{1}{2^{1/2}} \left(T^p \hat{\beta} + T^m \left[\sin\alpha_0 + T^{1+p} \frac{\beta}{1+p} \cos\alpha_0 \right] \right). \tag{5.28}$$

We again consider three cases:

(*a*) $p < m$: Suppose the plate rotation power law is less than that for plate translation, i.e. $p < m$, and recall that $m, p \geq 0$. Then from (5.28), dominant balance gives $s = q/2 + p$. The T power laws of the second and third terms in (4.4) are both $-q/2 + p$. A dominant balance between the left-hand side of (4.4) and these two terms now gives $q = 2(p+1)/3$ and $s = (4p+1)/3$. Thus, the T^m term in $\tilde{Q}$ in (4.5*b*) is subdominant. The first term on the right-hand side of (4.4) again is always subdominant for $m > 0$. This case is identical to (5.6) and (5.7) (zero initial angle of attack) and gives a Type I vortex sheet, i.e. the start-up motion is rotation dominated.

(*b*) $p > m$: Now consider the opposite case. From (5.28), the first term on its right-hand side is subdominant, giving $s = q/2 + m$. The T power-laws of the second and third terms on the right-hand side of (4.4) are both $-q/2 + m$. A dominant balance between the left-hand side of (4.4) and these two terms then gives $q = 2(m+1)/3$ and $s = (4m+1)/3$; the first term on its right-hand side is always subdominant for $m > 0$. This case is identical to (5.6) and (5.7) with p and $\hat{\beta}$ replaced by m and $\sin\alpha_0$, respectively. This gives a Type I vortex sheet, but one that is convection dominated due to non-zero angle of attack (rather than rotation dominated). This is equivalent to a start-up flow with no plate rotation, $\hat{\beta} = 0$, and non-zero angle of attack, $\alpha_0 > 0$ (Pullin 1978).

(*c*) $p = m$: This case is delicate, and we first consider $\hat{\beta} + \sin\alpha_0 \neq 0$. The T^{1+p} term on the right-hand side of (5.28) is subdominant. Both surviving terms on the right-hand side of (5.28) balance while the term proportional to T^m in (4.4) remains subdominant. This is the same as $p < m$ in case (*a*) above with $\hat{\beta}$ replaced by $\hat{\beta} + \sin\alpha_0$, i.e. a Type I vortex sheet that arises from a balance between convection and rotation. As a parameter point in (m, p) space crosses the line $m = p$, the T power laws and the Type I vortex sheet solution are continuous. However, $Z(\lambda)$ will always be twice discontinuous and the dominant physics will change from rotation-dominated (case (*a*)) to rotation-convection balanced (this case) to convection dominated (case (*b*)).

Next, we study $p = m$ but now with $\hat{\beta} + \sin\alpha_0 = 0$. Here, the right-hand side of (5.28) and $\tilde{Q}$ in (4.5*b*) are proportional to T^{1+2p}, to leading order. Equation (5.28) then gives, $s = q/2 + 2p + 1$. Now consider a dominant balance between the left-hand side and the second and third terms of (4.4). A short calculation gives

$$q = \tfrac{4}{3}(1+p), \tag{5.29}$$

and $s = (5+8p)/3$. For the convective (first) term on the right-hand side of (4.4) to be subdominant relative to its left-hand side, we require $p > q - 1$. Substituting (5.29) into this inequality then gives $p < -1$, which violates the overriding constraint, $p \geq 0$,

in (2.10*a*,*b*). Hence, these solutions do not exist. The other possibility is a balance between the left-hand side and the convective term on the right-hand side of (4.4). This gives $q = 1 + p$ and $s = (3 + 5p)/2$, leading to a Type II convective-dominated starting vortex. This is the exceptional case where a Type II solution exists for $\alpha_0 \neq 0$.

5.4. $\alpha_0 \neq 0$, $d = 1/2$

Finally, we study $d = 1/2$ where the rotation pivot is at the three-quarter chord point, with non-zero initial angle of attack, $\alpha_0 \neq 0$. Here, the second terms in the arguments of the $\cos\alpha(t)$ and $\sin\alpha(t)$ in (4.4) and (4.5*b*), respectively, can be neglected for $T \ll 1$ while the term, $T^p\beta(1/2 - d)$, in (4.5*b*) is zero. Equations (4.4) and (4.5*b*) then become

$$T^{q-1}\left(q\bar{Z} + s(1-\lambda)\frac{\mathrm{d}\bar{Z}}{\mathrm{d}\lambda}\right) = T^m\cos\alpha_0 - T^{-(q/2)+m}\frac{\mathrm{i}}{Z^{1/2}}\left(\frac{1}{2^{1/2}}\sin\alpha_0 + \frac{\mathcal{J}}{4\pi}I(Z)\right), \tag{5.30a}$$

$$\frac{\mathcal{J}}{4\pi}T^{s-(q/2)}\int_0^1\left(\frac{1}{Z^{1/2}} + \frac{1}{\bar{Z}^{1/2}}\right)\mathrm{d}\lambda = \frac{1}{2^{1/2}}T^m\sin\alpha_0. \tag{5.30b}$$

From (5.30*b*), finite shed circulation requires $s = q/2 + m$. We seek a dominant balance between the left-hand side and the (rotational) second and third terms on the right-hand side of (5.30*a*), which gives $q = 2(1 + m)/3$ and $s = (4m + 1)/3$. A subdominant first term on the right-hand side of (5.30*a*) requires $m > q - 1$, which upon substitution of the preceding expression for q, gives $m > -1$. This inequality is always satisfied since $m \geq 0$; see (2.10*a*,*b*). The resulting equations are identical to (5.5*a*,*b*) and (5.6) with p and $\hat{\beta}$ replaced by m and $\sin\alpha_0$, respectively. This is again a Type I vortex sheet, but is convection dominated due to non-zero initial angle of attack. There exists no solution with a dominant balance between the left-hand side and (convective) first term on the right-hand side of (5.30*a*). This would require $q = 1 + m$ while a subdominant second-third term on the right-hand side needs $q < 0$. These two expressions for q imply that $m < -2$ which is not allowed, notwithstanding that $q \geq 0$ is required; see (4.1*a*,*b*).

5.5. *Summary of vortex types*

Table 1 summarizes the results of the analyses in §§ 5.1–5.4, the key points of which are:

(*a*) Type I vortex sheets appear in each of the four distinct plate motions, for certain parameter ranges.
(*b*) Type II vortex sheets are restricted to zero initial angle of attack, $\alpha_0 = 0$, over certain parts of the (m, p) plane, and also to $\alpha_0 \neq 0$ under the condition that both, $m = p$, and, $\hat{\beta} + \sin\alpha_0 = 0$.
(*c*) Type III sheets appear only for zero initial angle of attack, $\alpha_0 = 0$, along the lines (i) $m = 1 + 2p$ for plate rotation about its three-quarter chord position, $d = 1/2$, and (ii) $m = (2p - 1)/3$ for $d \neq 1/2$.

The right-hand column of table 1 indicates the dominant physics that control the starting vortex for each of the eleven flow regimes shown. Type I vortex sheets appear for both strict rotation and convection-dominated flows, and in one case for a combination of rotation and convection. Type II sheets occur only for convection dominated starting vortices.

Plate orientation and pivot position	Plate power-laws	Type	Vortex, q	Vortex, s	Physics
$\alpha_0 = 0, d \neq \frac{1}{2}$	$m > \frac{1}{3}(2p-1)$	I	$\frac{2}{3}(1+p)$	$\frac{1}{3}(1+4p)$	Rotation
	$m = \frac{1}{3}(2p-1)$	III	$\frac{2}{3}(1+p)$	$\frac{1}{3}(1+4p)$	Rotation–convection
	$m < \frac{1}{3}(2p-1)$	II	$1+m$	$p+\frac{1}{2}(1+m)$	Convection
$\alpha_0 = 0, d = \frac{1}{2}$	$m > 1+2p$	I	$\frac{2}{3}(2+m+p)$	$\frac{1}{3}(5+4m+4p)$	Rotation
	$m = 1+2p$	III	$2(1+p)$	$3+4p$	Rotation–convection
	$m < 1+2p$	II	$1+m$	$p+\frac{3}{2}(1+m)$	Convection
$\alpha_0 \neq 0,\ d \neq \frac{1}{2}$	$m > p$	I	$\frac{2}{3}(1+p)$	$\frac{1}{3}(1+4p)$	Rotation
	$m = p$ $(\hat{\beta} + \sin\alpha_0 \neq 0)$	I	$\frac{2}{3}(1+p)$	$\frac{1}{3}(1+4p)$	Rotation–convection
	$m = p$ $(\hat{\beta} + \sin\alpha_0 = 0)$	II	$1+p$	$\frac{1}{2}(3+5p)$	Convection
	$m < p$	I	$\frac{2}{3}(1+m)$	$\frac{1}{3}(1+4m)$	Convection
$\alpha_0 \neq 0, d = \frac{1}{2}$	All	I	$\frac{2}{3}(1+m)$	$\frac{1}{3}(1+4m)$	Convection

TABLE 1. Summary of vortex sheets and time power laws, $q \geq 0$ and $s \geq 0$, of their similarity solutions in (4.1*a*,*b*) for each of the four dominant plate motions. Plate motion is specified by four control parameters: initial angle of attack, α_0, plate pivot position, d, and time power laws, $m \geq 0$ and $p \geq 0$, for the plate translational and rotational speeds, respectively; see (2.1), (2.10*a*,*b*) and (2.12). The far right column summarizes the dominant flow physics for each vortex sheet.

Because Type III vortex sheets describe a transition regime, these are always controlled by a mix of rotation and convection.

5.6. *Vanishing plate rotation and degenerate vortex sheets*

The present theory assumes the plate always rotates, i.e. $\Omega_0 > 0$ and hence $\beta > 0$. It is also of interest to study the limit of vanishing plate rotation, i.e. $\alpha(t) = \alpha_0 = \text{constant}$, because this can align with problems of practical interest. For example, the widely studied start-up of a flat plate at constant translational speed and fixed non-zero angle of attack (Prandtl 1924). Interestingly, some starting vortices in table 1 present singular solutions for vanishing plate rotation, i.e. the limit $\beta \to 0^+$ differs from $\beta = 0$, while others are continuous. Thus, care must be taken when applying such singular configurations in a practical setting, because even a small amount of rotation can potentially change the resulting shed (primitive) vortex.

We provide two examples for fixed non-zero angle of attack, $\alpha(t) = \alpha_0 > 0$:

(*a*) Consider the above-mentioned flow of a plate moving with impulsive and constant translational speed, $m = 0$ (Prandtl 1924). Regardless of the plate rotation power law, $p \geq 0$, table 1 shows that a Type I vortex sheet arises with vortex power law, $q = 2/3$, as the plate rotation speeds approaches zero, i.e. $\beta \to 0^+$. This vortex power law of 2/3 is identical to the result for identically zero rotation; see page 414 of Pullin (1978), who studied a semi-infinite plate, the results of which are

applicable here because the leading edge of a finite plate does not affect its primitive trailing-edge vortex; see § 1. That is, the solution is continuous in the limit, $\beta \to 0^+$.

(*b*) Next, we study the related problem of a plate undergoing constant acceleration, $m = 1$, with the rotation pivot point away from the three-quarter chord position, $d \neq 1/2$. If the plate rotation power law, $p < m\ (= 1)$, table 1 shows that a Type I (rotation dominated) vortex sheet emerges with a vortex power-law of $q = (2/3)(1 + p)$, as $\beta \to 0^+$. Thus, even though the plate angular speed approaches zero, the vortex dynamics is still intimately controlled by plate rotation. In contrast, if $p > m\ (= 1)$, a Type I (convection dominated) vortex sheet emerges with a vortex power law of $q = 4/3$, i.e. the vortex dynamics is independent of plate rotation; the same vortex power law holds for $p = m\ (= 1)$. Consequently, vortex dynamics from this plate motion exhibits singular behaviour: (i) the limit of infinitesimal plate rotation, $\beta \to 0^+$, depends on the plate rotation power-law, p, while (ii) identically zero plate rotation, $\beta = 0$, is by definition independent of p.

This degeneracy in these (inviscid) vortex dynamics is likely resolved in a practical setting through the influence of viscosity. The same holds for any degeneracy that may be encountered for vanishing plate translation. These remain open questions.

6. Behaviour in the time domain

In this section, we provide sample vortex sheets in the time domain to facilitate future comparison to high Reynolds number flows of the predicted phenomena. These highlight (i) nascent vortex growth on the (laboratory) spatial scale of the plate half-chord, and (ii) vortex sheet type transition. It is emphasized that the present study focuses on asymptotic solutions for small times, i.e. the 'primitive start-up vortex sheet'. Since the vortex sheets are shown as a function of time, and hence of finite spatial size, some may go beyond this strict asymptotic range of validity. Even so, they may be used to guide experiments or viscous flow simulations that aim to test the theoretical predictions reported.

We focus on vortex sheets produced by the first distinct plate motion, studied in § 5.1: zero initial angle of attack, $\alpha_0 = 0$, and pivot point away from the three-quarter chord position of the plate, i.e. $d \neq 1/2$. We also specify that the plate translates impulsively with uniform acceleration, $m = 1$. The plate rotation power-law, p, is varied to span the VST point at $p = (3m + 1)/2$, which for $m = 1$ gives $p = 2$; where a transition from Type I to Type III to Type II occurs. All sample flows show the vortex centre of roll-up moving in a straight line trajectory, a fundamental property that follows directly from the similarity solution in (4.1*a*,*b*); time, T, simply increases the magnitude of the vortex coordinates, $\hat{z}_v$, about the plate trailing edge (without changing the vortex shape). Moreover, the vortex size and position depend on the rotation-to-translation parameter, $\hat{\beta}$, dimensionless time, T and plate rotational power law, p. Results are provided in the moving reference frame of the plate (not the laboratory frame), and are independent of the rotation pivot position.

Type I vortex sheet ($p < 2$). In figure 10, we show the vortex development for $p = 1$ for several small convective times, T, which corresponds to uniform rotational acceleration of the plate. A rotation-dominated Type I vortex-sheet results, whose shape is identical to figure 4(*b*); the vortex cores move at an angle of 111.3° to the positive x axis, which is independent of $\hat{\beta}$. While the vortex shape is independent of the rotation parameter, $\hat{\beta}$, its

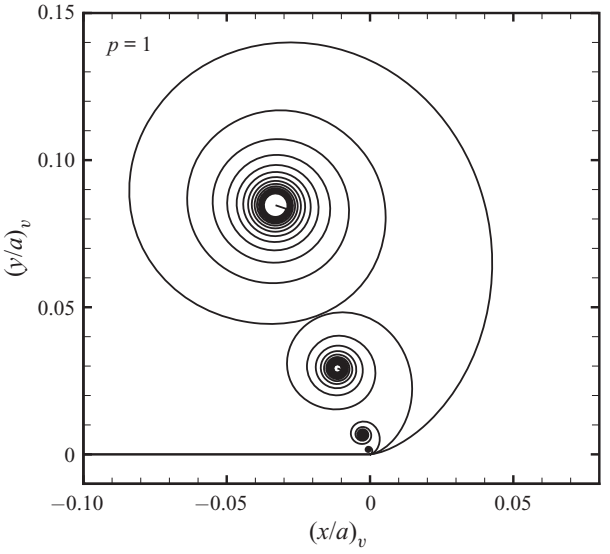

FIGURE 10. Time series showing Type I vortex-sheet evolution, in moving reference frame of the plate. Zero initial angle of attack, $\alpha_0 = 0$, constant translational plate acceleration, $m = 1$, and constant plate rotational acceleration, $p = 1$. Times series corresponds to $T = 0.0158$, 0.0474, 0.1423, 0.3162 for $\hat{\beta} = 5$, which are identical to $T = 0.05$, 0.015, 0.45 and 1 for $\hat{\beta} = 0.5$, respectively. Time series are independent of the plate pivot position, provided $d \neq 1/2$. The vortex centre trajectory makes an angle if 111.3° with the positive x-axis. This angle depends only on p.

time evolution depends strongly on $\hat{\beta}$. The vortex size and position grow as $\hat{\beta}^{2/3}T^{4/3}$, and the effect of varying $\hat{\beta}$ is illustrated in the caption of figure 10. Specifically, the vortices in figure 10 occur at $T = 0.05$, 0.015, 0.45, 1 for $\hat{\beta} = 0.5$, while the same vortex time series is recovered for $\hat{\beta} = 5$ with $T = 0.0158$, 0.0474, 0.1423, 0.3162, respectively. In all cases, the vortex size remains much smaller than the plate span, $2a$, while being of a significant (observable) size. This suggests that the time-series similarity predicted for the two sets of $(\hat{\beta}, \{T\})$ parameters in figure 10 should be testable experimentally or via simulation.

Type III vortex sheet ($p = 2$). Figure 11 gives time series for Type III vortex sheets that occur at the VST point, $p = 2$. Both the vortex core position and its spatial size now vary as $\hat{\beta}^{2/3}T^2$, and so the vortex growth is slow relative to the Type I vortex sheet in figure 10. As discussed in § 5.1.4, this vortex type depends strongly on the rotation-to-translation parameter, $\hat{\beta}$. Results for $\hat{\beta} = 5$ are shown in figure 11(a). Here, the starting-vortex centre or edge trajectory is just outboard of the normal to the plate trailing edge, with the core trajectory at an angle of 81.5° to the positive x axis. Complementary time series for $\hat{\beta} = 0.5$ are provided in figure 11(b). Owing to the decreasing effect of rotation and the increasing influence of convection as $\hat{\beta}$ decreases, the vortex structure becomes stretched with a rolled-up core that is more compact than for $\hat{\beta} = 5$; the core trajectory is more aligned with the translational flow, and now makes an angle of 24.6° to the plate. Again, the spatial extent of the vortices are small relative to the plate span, but of sufficient size to be observed, facilitating their measurement.

Type II vortex sheet ($p > 2$). Here, the vortex sheet is parallel to the plate (even as it rotates). Its (free) downstream edge position is given by (5.12a,b) and (5.15a) with $\lambda = 1$: $\hat{z}_v|_{edge} = aT^2/2$ and is independent of both p and $\hat{\beta}$. Choosing a dimensionless convective

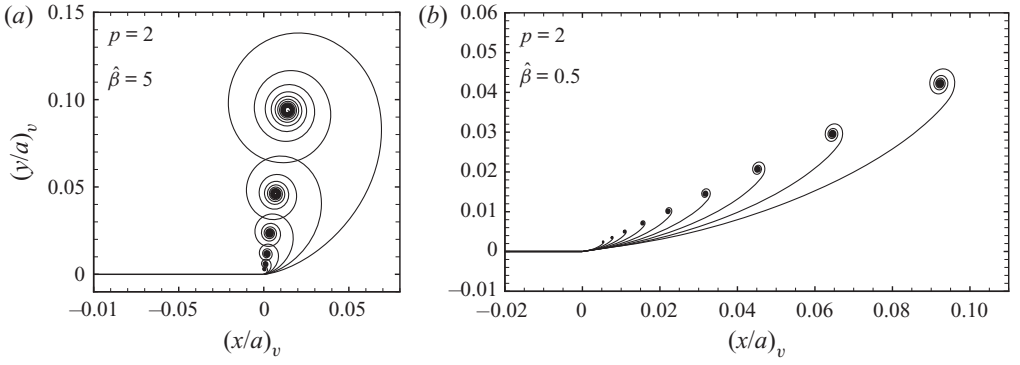

FIGURE 11. Time series showing Type III vortex-sheet evolution, in moving reference frame of the plate. Plate control parameters, $\alpha_0 = 0$ and $m = 1$, as for figure 10, except that the plate rotation power law is now at the VST point, $p = (3m + 1)/2 = 2$. (*a*) $\hat{\beta} = 5$ with $T = 0.0084$, 0.125, 0.0177, 0.25, 0.354, 0.5; vortex core at 81.5° to the positive x axis. (*b*) $\hat{\beta} = 0.5$ with $T = 0.1021$, 0.1435, 0.1715, 0.0205, 0.245, 0.2928, 0.35, 0.418, 0.5; vortex core at 24.6° to the positive x axis. Both time series are independent of the plate pivot position, provided $d \neq 1/2$.

time, $T \ll 1$, in measurements ensures the vortex-sheet length is small relative to the plate span, allowing for comparison using this simple formula for $\hat{z}_v|_{edge}$.

7. Effect of finite Reynolds number

In this section, we examine the effect of viscosity, i.e. finite Reynolds number, on the presented inviscid calculations. We focus on Type I and II vortex sheets, since they arguably present the most interesting flow structures.

7.1. *Type I vortex sheet*

We first study Type I vortex sheets that are rotation dominated. A similar analysis for other Type I solutions is straightforward. Near the leading edge of the flat plate, the outer inviscid complex potential follows from (2.8),

$$W(\hat{z}, t) = -\mathrm{i}At^p\hat{z}^{1/2} + \cdots, \tag{7.1}$$

where $A = D(a/2)^{3/2}\Omega_0(U_0/a)^p$ and $D = 1/2 - d$. The dimensions of A are length$^{3/2}$ × time$^{-(1+p)}$.

Consider some point-wise quantity that characterizes the vortex growth, such as the (dimensional) centre of a vorticity distribution, $\hat{z}_c$. Because vorticity takes finite time to diffuse from the plate, the outer flow remains essentially inviscid during the early-time viscous vortex growth. It is then assumed that for a viscous flow at sufficiently small times, where the starting vortex remains close to the leading edge, the dependence of $\hat{z}_c$ on the plate and flow parameters takes the functional form

$$\hat{z}_c = \hat{z}_c(A, t, \nu \,|\, p), \tag{7.2}$$

where ν is the kinematic viscosity of the fluid. That is, the vorticity distribution centre depends on the rotational power law, p, but not the translational power law, m;

see (2.10*a*,*b*). Dimensional analysis then gives

$$\frac{\hat{z}_c}{A^{2/3}t^{(2/3)(1+p)}} = F(Re_t \,|\, p), \tag{7.3}$$

where $F(Re_t \,|\, p)$ is a dimensionless function (to be determined), and

$$Re_t = \frac{A^{4/3}t^{(1/3)(1+4p)}}{\nu}, \tag{7.4}$$

is a time-dependent Reynolds number.

For the shed circulation, Γ_s, at time, t, a similar analysis gives

$$\Gamma_s = A^{4/3}t^{(1/3)(1+4p)}G(Re_t \,|\, p), \tag{7.5}$$

where $G(Re_t \,|\, p)$ is another dimensionless function. From (4.1*a*,*b*), the vorticity distribution centre is given by $\hat{z}_c = \hat{z}_v(\lambda = 1, t)$, corresponding to the centre of the inviscid vortex roll up. Equations (5.5*a*,*b*) and (5.9*a*,*b*) then give

$$F(Re_t \,|\, p) = \left(\frac{3}{1+p}\right)^{2/3} \omega(\lambda = 1, p), \tag{7.6a}$$

$$G(Re_t \,|\, p) = 4J(p)\left(\frac{3}{1+p}\right)^{1/3}, \tag{7.6b}$$

which are both independent of Re_t, where $J(p)$ is defined in (5.8*a*,*b*).

For the rotation-dominated Type I vortex considered here, Re_t is related to the plate Reynolds number, $Re_c \equiv 2aU_0/\nu$, by

$$Re_t = Re_c \tfrac{1}{8}\hat{\beta}^{4/3}T^{(1/3)(1+4p)}. \tag{7.7}$$

Two limits are of practical interest:

(*a*) $Re_c \to \infty$ at fixed and finite T. Equation (7.7) then gives $Re_t \to \infty$, i.e. both Reynolds numbers are infinite. A reasonable but unproven hypothesis is that this limit would produce a turbulent starting vortex whose structure may or may not be related to the present inviscid similarity solution.

(*b*) $Re_c \to \infty$ and $T \to 0$ such that Re_t is fixed and moderately large. Importantly, inviscid theory finds support from experiment and viscous simulation for moderately large Re_c and Re_t. For example, figure 4(*e*) of Pullin & Perry (1980) shows reasonable agreement between experiment and the inviscid theory (for z_c) for wedges and thin plates with $Re_t \sim 10^3$–10^6. Similarly, Xu *et al.* (2017) report good agreement between viscous and inviscid solutions for the location, size and shape of the vorticity spiral vortex cores, and also for the shed circulation as a function of time, for $Re_c = 250$–2000. These previous studies suggest that similar agreement may be found for the present problem in this limit of very small convective time, $T \ll 1$, at moderately large Re_t.

7.2. *Type II vortex sheet*

For a Type II, convection-dominated vortex sheet, (7.2) is replaced by

$$\hat{z}_e = \hat{z}_e(a, U_0, t, \nu \,|\, p, m), \tag{7.8}$$

where $\hat{z}_e$ refers to the free end of the sheet. That is, the solution depends on both the translational and rotational power laws, m and p, respectively. Dimensional analysis then gives

$$\frac{\hat{z}_e}{a} = H(T, Re_t \,|\, p, m), \qquad \frac{\Gamma_s}{U_0\, a} = M(T, Re_t \,|\, p, m), \tag{7.9a,b}$$

where $H(T, Re_t \,|\, p, m)$ and $M(T, Re_t \,|\, p, m)$ are dimensionless functions, and

$$Re_t = Re_c \frac{T}{2}. \tag{7.10}$$

From § 5.1.3, we then find

$$H(T, Re_t \,|\, p, m) = \frac{1}{1+m} T^{1+m}, \quad M(T, Re_t \,|\, p, m) = \mathcal{J}\, T^{p+((1+m)/2)}, \tag{7.11a,b}$$

which are again independent of Re_t. A large Reynolds number limit analysis can be performed, as for the Type I vortex sheet; this is left to the reader.

Experiments or viscous-resolved computational simulations that could distinguish the formation Type I or Type II structures in the $(m - p)$ plane for moderate Re_t would seem feasible.

8. Summary and conclusion

We have considered the primitive trailing-edge vortex produced by the start-up motion of a flat plate in a inviscid fluid; see figure 1. The plate moves with a time power-law translational speed of exponent, $m \geq 0$, while simultaneously undergoing a clockwise angular speed with time power law, $p \geq 0$; see (2.10*a*,*b*). This rotation is about a pivot point on the plate, whose position is specified by a dimensionless constant, d; see (2.1). The plate motion is also specified by its initial angle of attack, α_0; see (2.12). The dimensionless constant, $\beta > 0$, characterizes the relative strength of plate rotation to translation; see (2.13).

For almost all combinations of these parameters, there exists for $T = 0^+$, a singularity of the attached flow at the plate trailing edge. The exception is the limit of zero angle of attack and zero rotation, i.e. $\alpha(t) \to 0$ and $\Omega_0 \to 0$, respectively, for which the plate motion does not disturb the fluid.

The appearance of an attached-flow singularity at the plate trailing edge is resolved by the generation of a nascent vortex in the form of a separating vortex sheet, of *a priori* unknown structure. A Birkhoff–Rott equation is formulated, together with an associated Kutta condition that ensures finite velocity at this trailing edge, that describes the sheet motion. The resulting equations admit similarity solutions for the primitive vortex – for small time via dominant-balance analysis – that represents both the sheet profile shape and the rate at which circulation is shed at the plate trailing edge. In so doing, the Birkhoff–Rott equation contracts to either a nonlinear integral-differential equation or to a linear ordinary differential equation, with the Kutta condition providing an integral constraint.

Vortex-sheet solutions are classified into three distinct types according to the contracted form of the Birkhoff–Rott equation:

Type I represents separation with a strong rolled-up vortex of spatial extent given by the distance of its centre to the plate trailing edge. Its centre moves approximately normal to the plate. Where Type I vortex sheets appear, they can always be mapped to special cases of known self-similar solutions (Pullin 1978). Their equivalent point-vortex representations correspond to solutions obtained by Rott (1956). Type I vortex sheets occur for all plate motion power laws, $m, p \geq 0$, when the initial angle of attack is non-zero, $\alpha_0 > 0$; but only for a subset of m and p when $\alpha_0 = 0$. They appear typically for (i) strong plate rotation, regardless of the initial angle of attack, α_0, and (ii) for $\alpha_0 > 0$ when translational convection dominates.

Type II vortex sheets are strictly convection dominated and appear when $\alpha_0 = 0$, and also under special circumstances for $\alpha_0 > 0$. Here, self-induction of the vortex sheet is negligible compared with the local translational convection velocity near the plate edge. The consequence is that the sheet is always flat and parallel to the plate at the trailing edge – it rotates as a rigid body in tandem with the plate. Exact analytical solutions are found for these cases. Type I and II vortex sheets dominate the (m, p) space.

Type III sheets occur only for zero initial angle of attack, $\alpha_0 = 0$, along (singular) straight lines in the (m, p) plane. These lines divide Type I and II solutions. These vortex sheets arise from a dynamic balance between translational convection and vortex self-induction. As the plate control parameters are varied to cross these straight lines, the nascent vortex solution is generally twice discontinuous, with a singular solution occurring at the straight line. Even so, the vortex sheet is well defined for any set of given plate control parameters.

Type III vortex sheets match their Type I and II counterparts in the respective limits of $\beta \to \infty$ and 0, where plate rotation and translation dominate, respectively.

The asymptotic limit of zero plate rotation was also explored. Some plate motions were found to be not continuous relative to identically zero plate rotation, i.e. fixed angle of attack, $\alpha(t) = \alpha_0 =$ constant. That is, the asymptotic limit of zero plate rotation is singular. Resolution of this intriguing behaviour may lie in the inclusion of viscous effects, which represents an avenue for future work. Similarly, viscosity may also affect other singular behaviour exhibited in this inviscid formulation, such as the linear boundaries in (m, p) space along which Type III vortex sheets occur.

Finally, we emphasize that existence of these inviscid solution types as appropriate moderate to high Reynolds number limits of viscous, flat-plate starting flows remains an open question. In §§ 6 and 7, we presented a set of flow parameters, time series of vortex motions and viscous flow analysis that can be used for comparison to address this important issue.

Acknowledgements

The authors thank T. Colonius and T. Leonard for stimulating discussion. J.E.S. acknowledges support from the Australian Research Council Centre of Excellence in Exciton Science (CE170100026) and the Australian Research Council grants scheme.

Appendix. Convergence of numerical method

In this appendix, we present a convergence study of the numerical method discussed in § 5.1.2. A refinement study as a function of N is performed for a Type I vortex sheet with $p = 1$. CPU time per solution scales as N^3 owing to the required inversion of full

Case	N	Sheet turns	λ_N	J	Re$\{\omega_{N+1}\}$	Im$\{\omega_{N+1}\}$
A	1220	15	0.974544	2.24123	−0.126782	0.325594
B	2440	15	0.974262	2.24207	−0.126683	0.325730
C	2400	33	0.992301	2.24122	−0.126897	0.325390
D	4800	33	0.992178	2.24206	−0.126799	0.325526

TABLE 2. Numerical results showing the effect of discretization refinement on the rescaled shed circulation constant, J, and position of the vortex centre in the ω-plane, ω_{N+1}. Four cases are shown for a Type I vortex sheet with $p = 1$.

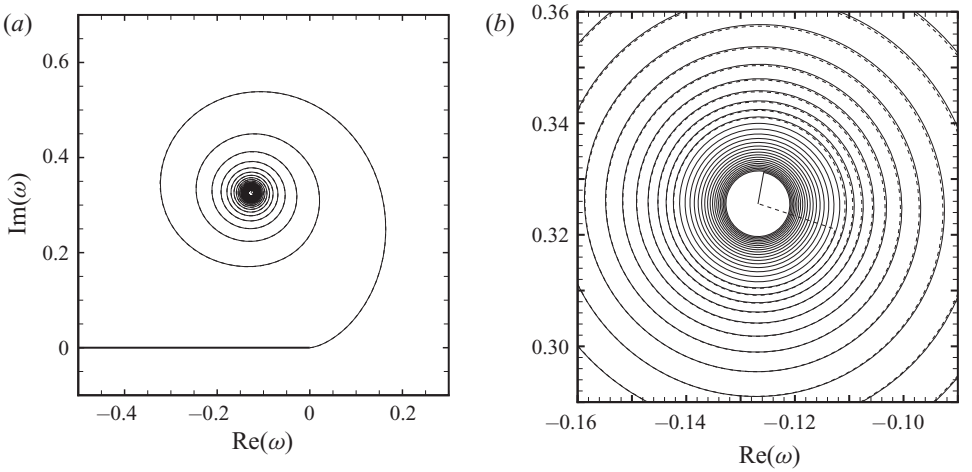

FIGURE 12. Numerical solution of Type I vortex sheet, $p = 1$, with coarsest and finest level of discretization corresponding to Cases A and D in table 2, respectively. Case A (dashed line) and Case D (solid line). (*a*) Complete vortex sheet. (*b*) Close up of core showing tightly wound sheet profiles.

but generally well-conditioned Jacobian matrices at each stage of the Newton–Raphson solution method. All solutions shown have averaged residuals of approximately 10^{-14}. Four different cases are shown in table 2.

Case Afighere fig13 of table 2 is a vortex sheet with 15 sheet turns, i.e. the vortex winds around its core 15 times, with 60–90 points per sheet turn, giving $N = 1220$. Case B uses the same number of turns with double the discretization, N. Cases C and D have double the number of sheet turns and double the N-values as Cases A and B, respectively, and thus use identical discretizations. For the main solution parameters, the rescaled shed circulation constant, J, and position of the vortex centre in the ω-plane, ω_{N+1}, table 2 shows that doubling the discretization produces differences in the fourth significant figure. The majority of vortex-sheet solutions given this study thus use the Case A resolution level.

Figure 12 shows the calculated Type I vortex sheet ($p = 1$) in the ω-plane, for Cases A and D, that use the coarsest and finest levels of discretization, respectively. Any differences between Cases A and D are imperceptible on the global scale of the vortex sheet in figure 12(*a*). Expanding the scale of the vortex core as in figure 12(*b*), shows very slight differences between the two solutions. Note that the Case A vortex sheet stops winding at a larger radius than Case D, as expected since Case A uses only 15 sheet turns (as opposed

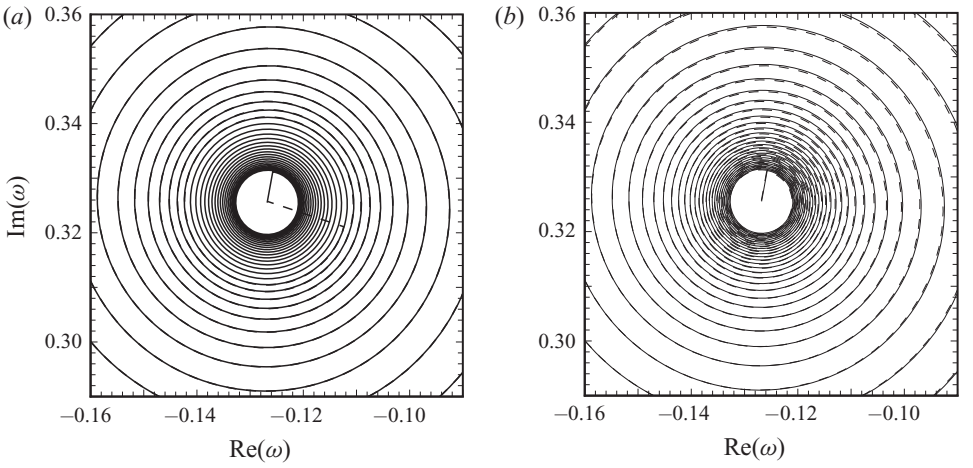

FIGURE 13. As for figure 12(*b*), but comparing Case D (finest discretization, solid line) to (*a*) Case B (dashed line) and (*b*) Case C (dashed line).

to 33 turns for Case D). Even so, the vortex core is well described by both Cases A and D, and differences between the two solutions away from the core are small.

Figure 13 compares the remaining Cases B and C, to Case D (finest discretization). Notably, Cases B and D are indistinguishable in figure 13(*a*) apart from the departure point from the sheet turns to the vortex core; the position of the core is identical in both Cases B and D. This is as expected because these solutions are specified by an initial value problem starting at $\lambda = 0$; using identical discretization must produce identical results up to the maximum value of λ chosen. Figure 13(*b*) shows that small differences occur between Cases C and D, which are similar to those reported in figure 12(*b*) (for Cases A and D). Again, this is expected because the levels of discretization used in Cases A and C are identical, as discussed above; the calculated core positions are identical.

REFERENCES

ANTON, L. 1939 Ausbildung eines wirbels an der kante einer platte. *Ing.-Arch.* **10** (6), 411–427.

ANTON, L. 1956 Formation of a vortex at the edge of a flat plate. *NACA Tech. Memo* 1398.

AUERBACH, D. 1987 Experiments on the trajectory and circulation of the starting vortex. *J. Fluid Mech.* **183**, 185–198.

BIRKHOFF, G. 1962 Helmholtz and Taylor instability. In *Proceedings of the Symp. Appl. Math.*, vol. 13, pp. 55–76.

BLENDERMANN, W. 1967 *Der Spiralwirbel am translatorisch bewegten Kreisbogenprofil: Struktur, Bewegung und Reaktion*. Institut für Schiffbau der Univ. Hamburg.

ELDREDGE, J. D. 2007 Numerical simulation of the fluid dynamics of 2D rigid body motion with the vortex particle method. *J. Comput. Phys.* **221** (2), 626–648.

GUIRAUD, J. P. & ZEYTOUNIAN, R. K. 1977 A double-scale investigation of the asymptotic structure of rolled-up vortex sheets. *J. Fluid Mech.* **79** (1), 93–112.

JONES, M. A. 2003 The separated flow of an inviscid fluid around a moving flat plate. *J. Fluid Mech.* **496**, 405–441.

KADEN, H. 1931 Aufwicklung einer unstabilen unstetigkeitsfläche. *Ing.-Arch.* **2** (2), 140–168.

KOUMOUTSAKOS, P. & SHIELS, D. 1996 Simulations of the viscous flow normal to an impulsively started and uniformly accelerated flat plate. *J. Fluid Mech.* **328**, 177–227.

KRASNY, R. 1991 Vortex sheet computations: roll-up, wakes, separation. *Lect. Appl. Maths* **28** (1), 385–401.

LUCHINI, P. & TOGNACCINI, R. 2002 The start-up vortex issuing from a semi-infinite flat plate. *J. Fluid Mech.* **455**, 175–193.

LUCHINI, P. & TOGNACCINI, R. 2017 Viscous and inviscid simulations of the start-up vortex. *J. Fluid Mech.* **813**, 53–69.

MICHELIN, S., SMITH, S. & LLEWELLYN, G. 2009 An unsteady point vortex method for coupled fluid–solid problems. *Theor. Comput. Fluid Dyn.* **23** (2), 127–153.

MILNE-THOMSON, L. M. 1996 *Theoretical Hydrodynamics*. Courier Corporation.

MOORE, D. W. 1975 The rolling up of a semi-infinite vortex sheet. *Proc. R. Soc. Lond.* A **345** (1642), 417–430.

NITSCHE, M. & XU, L. 2014 Circulation shedding in viscous starting flow past a flat plate. *Fluid Dyn. Res.* **46** (6), 061420.

PIERCE, D. 1961 Photographic evidence of the formation and growth of vorticity behind plates accelerated from rest in still air. *J. Fluid Mech.* **11** (3), 460–464.

PRANDTL, L. 1924 Über die entstehung von wirbeln in der idealen flüssigkeit, mit anwendung auf die tragflügeltheorie und andere aufgaben. In *Vorträge aus dem Gebiete der Hydro-und Aerodynamik (Innsbruck 1922)*, pp. 18–33. Springer.

PULLIN, D. I. 1978 The large-scale structure of unsteady self-similar rolled-up vortex sheets. *J. Fluid Mech.* **88** (3), 401–430.

PULLIN, D. I. & PERRY, A. E. 1980 Some flow visualization experiments on the starting vortex. *J. Fluid Mech.* **97** (2), 239–255.

PULLIN, D. I. & WANG, Z. J. 2004 Unsteady forces on an accelerating plate and application to hovering insect flight. *J. Fluid Mech.* **509**, 1–21.

ROTT, N. 1956 Diffraction of a weak shock with vortex generation. *J. Fluid Mech.* **1** (1), 111–128.

SAFFMAN, P. G. 1992 *Vortex Dynamics*. Cambridge University Press.

TCHIEU, A. A. & LEONARD, A. 2011 A discrete-vortex model for the arbitrary motion of a thin airfoil with fluidic control. *J. Fluids Struct.* **27** (5-6), 680–693.

WAGNER, H. 1925 Über die entstehung des dynamicshen auftriebes von tragflügeln. *Z. Angew. Math. Mech.* **5**, 17–35.

WEDEMEYER, E. 1961 Ausbildung eines wirbelpaares an den kanten einer platte. *Ing.-Arch.* **30** (3), 187–200.

XU, L. & NITSCHE, M. 2015 Start-up vortex flow past an accelerated flat plate. *Phys. Fluids* **27** (3), 033602.

XU, L., NITSCHE, M. & KRASNY, R. 2017 Computation of the starting vortex flow past a flat plate. *Proc. IUTAM* **20**, 136–143.